Università degli Studi di Ferrara
- Ex labore fructus -

INFN

New challenges in the spectral reconstruction of terrestrial gamma rays and reactor antineutrinos

Marica Baldoncini

Barcelona Supercomputing Center
Centro Nacional de Supercomputación

CAEN
Tools for Discovery

University of Maryland

CGT
Centro di GeoTecnologie
Università degli Studi di Siena

Supervisor: Prof. Fabio Mantovani

Ph.D. in Physics - Cycle XXIX - Ferrara 10 April 2017

Summary

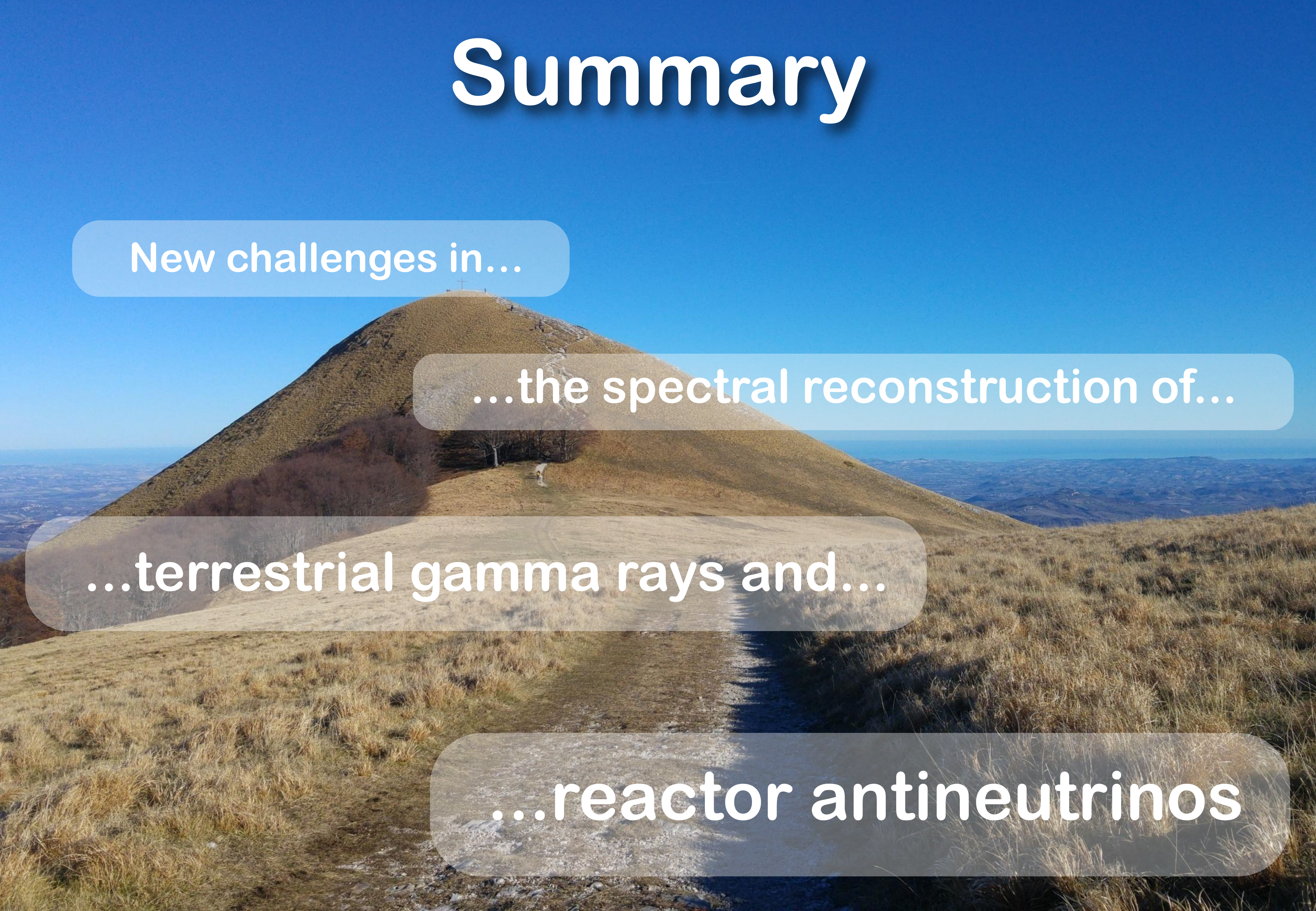
Summary
New challenges in...
...the spectral reconstruction of...
...terrestrial gamma rays and...
...reactor antineutrinos

Antineutrinos from reactors: a global view

✓Nuclear power plants are the strongest man made antineutrino sources (**L ~ 2 × 10^{20} $\overline{\nu}$/sec** for **1 GW** thermal power)

✓Liquid scintillation detectors: moving from the **Short BaseLine (SBL) (~1km)** and **Long BaseLine (LBL) era (~200 km)** towards the **Medium BaseLine (MBL) era (~50 km)**

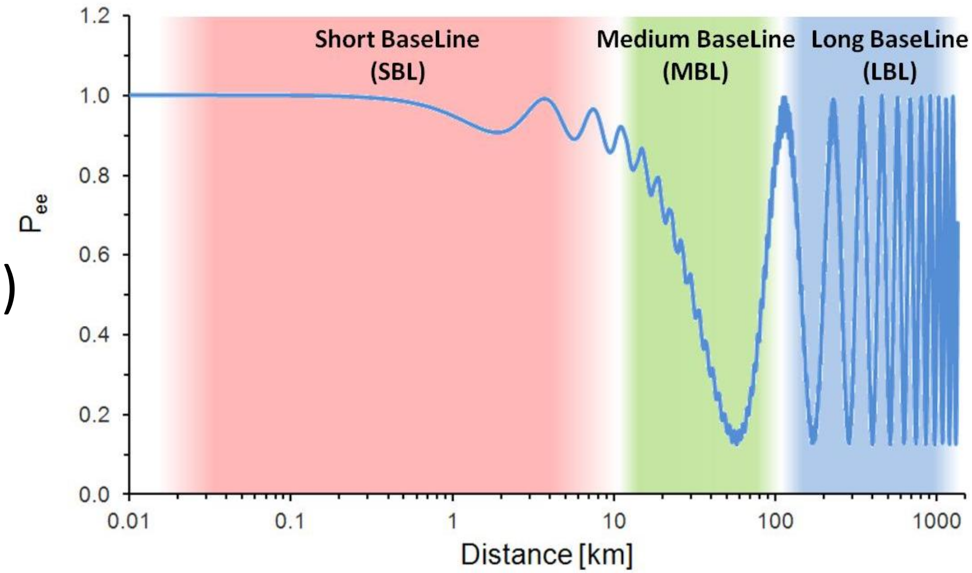

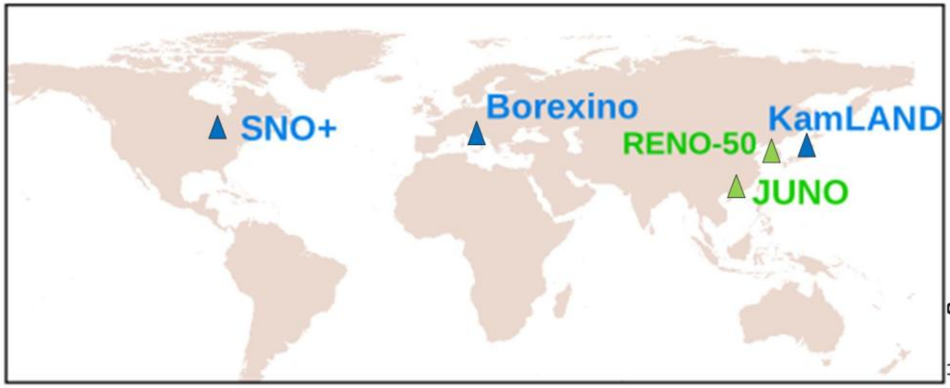

Goal of the work:

✓provide on the base of reactors official data a **worldwide reference model required** for estimating the reactor signal for **LBL experiments**

✓estimating **signal uncertainty** starting from the uncertainties on individual input quantities

Reactor antineutrinos: a fundamental background for geoneutrino measurements

Inverse **B**eta **D**ecay (**IBD**) Reaction

$$\bar{\nu}_e + p \rightarrow e^+ + n \; \mathbf{- 1.806\ MeV}$$

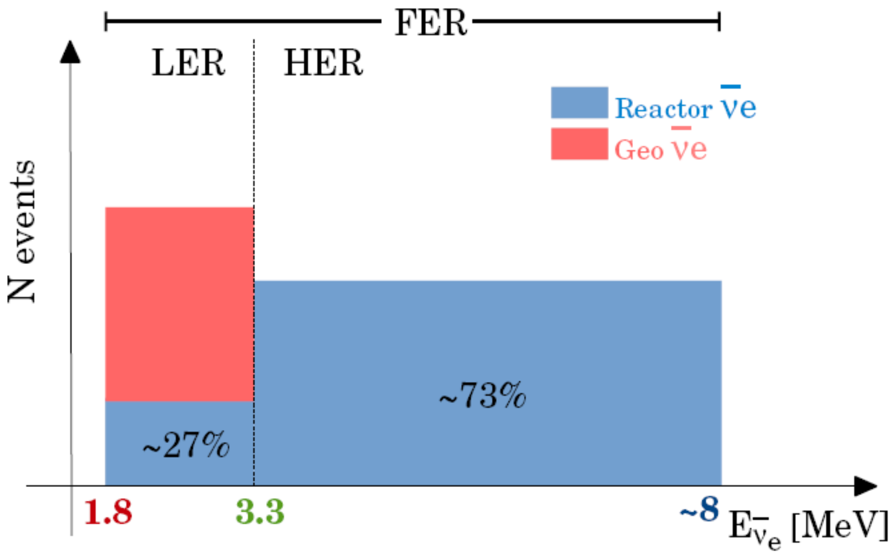

- ✓ **Low Energy Region (LER):** energy range starting at ***1.806 MeV*** (IBD threshold) and ending at ***3.3 MeV*** (end point of ^{214}Bi spectrum)
- ✓ **High Energy Region (HER)**: energy range starting at ***3.3 MeV*** and ending at ***8 MeV*** (end point of reactor spectrum)
- ✓ **Full Energy Region (FER) = LER + HER**

✓The ratio **r** between the reactor signal in the LER (**R**$_{LER}$) and the geoneutrino signal (**G**) **changes in time** according to the different reactor operational conditions

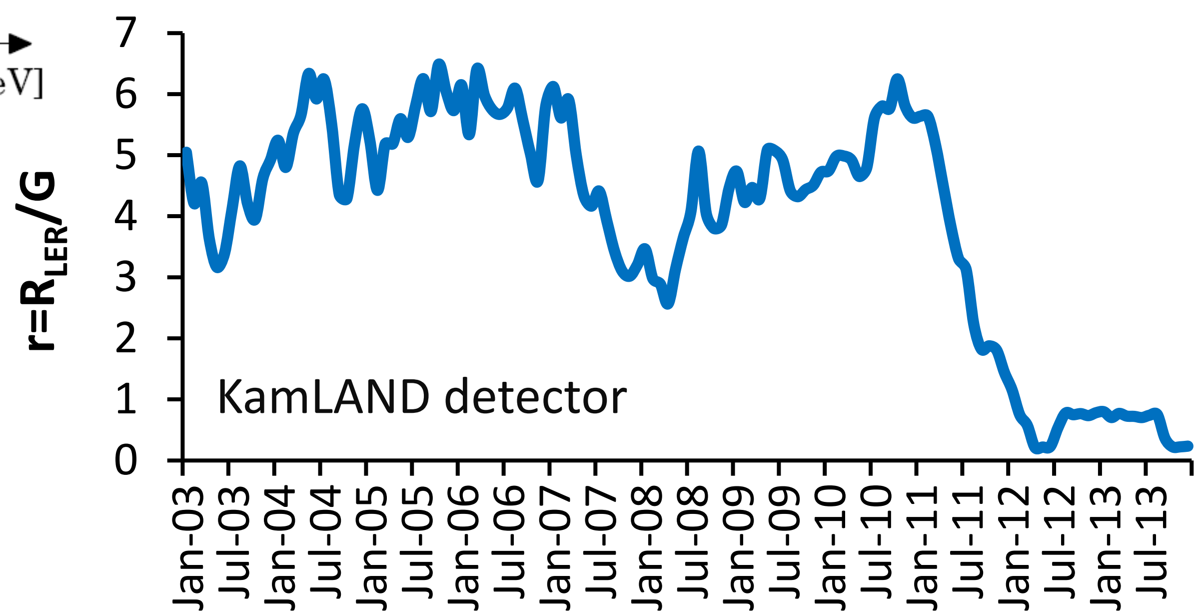

Reactor thermal power and fission fractions

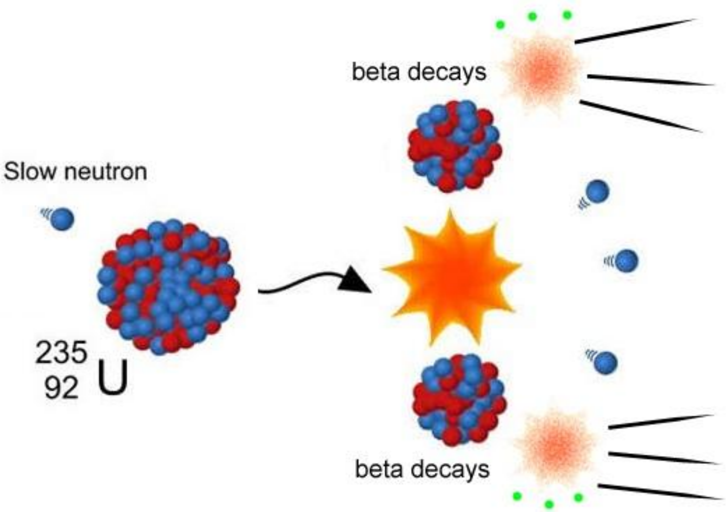

^{235}U, ^{238}U, ^{239}Pu, ^{241}Pu give **> 99%** of the fissions

A single fission process involves :

- the emission of **~ 6 antineutrinos**
- **~ 2 antineutrinos** above IBD threshold
- the production of **<Q> ~ 200 MeV**

$$P_{th} = R\sum_{i=1}^{4} f_i Q_i$$

R = total fission rate [fissions/sec]

f_i = relative fission yield, i.e the **fraction of fissions** produced by the *ith* isotope

Q_i **=energy released in one fission** of the *ith* isotope [MeV/fission]

~35% of commercial reactors has a P_{th} **~ 3GW**

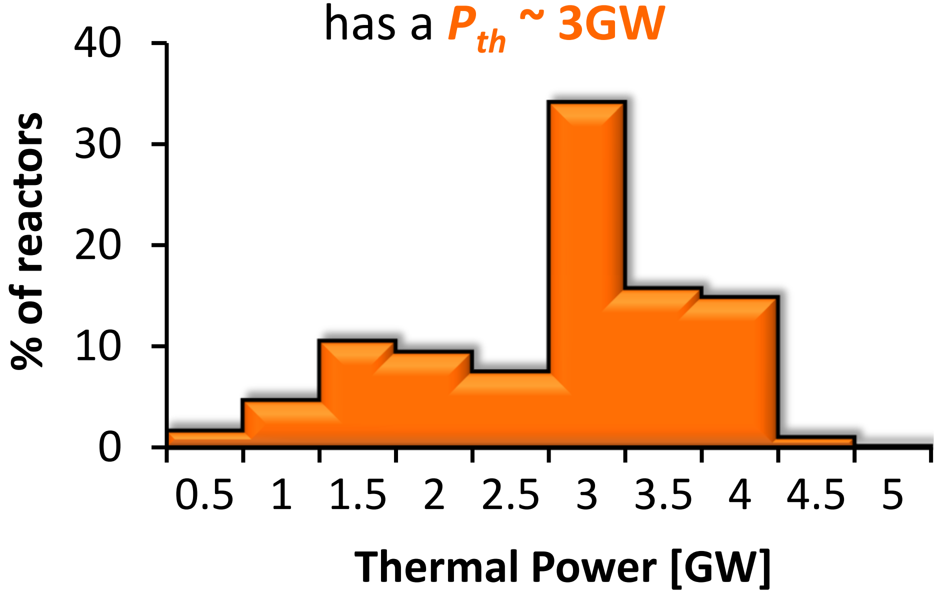

Fissile isotope	Q_i [MeV/fission]
^{235}U	202.36 ± 0.26
^{238}U	205.99 ± 0.52
^{239}Pu	211.12 ± 0.34
^{241}Pu	214.26 ± 0.33

Fission fractions and power fractions collection

$$p_i = \frac{f_i Q_i}{\sum_{i=1}^{4} f_i Q_i}$$

p_i is the **fraction of *P_{th}*** produced by the fission of the *ith* isotope

$$\frac{dN_i^{fiss}}{dt} = LF \cdot P_{th} \frac{p_i}{Q_i}$$

Extensive collection of different **sets of fission/power fractions** from literature

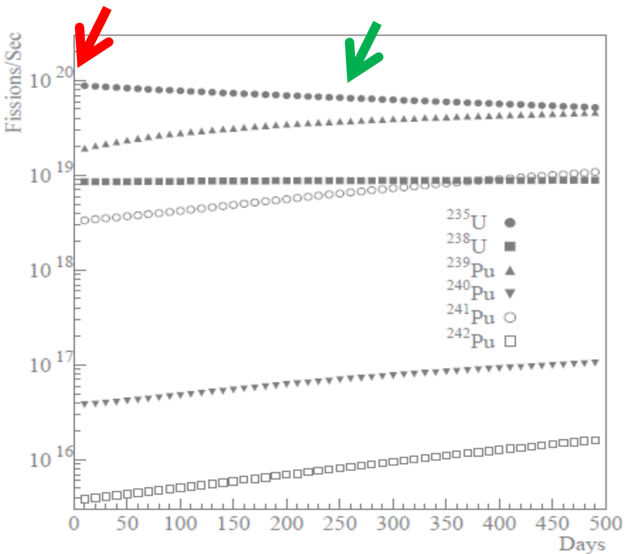

The values reported in the table depend on enrichment and burn up stage of the core

Reactor Classes	Fractions	^{235}U	^{239}Pu	^{241}Pu	^{238}U	Reference
		0.538	0.328	0.056	0.078	G. Mention et al. (2011)
		0.614	0.274	0.038	0.074	
		0.620	0.274	0.042	0.074	
		0.584	0.298	0.050	0.068	
		0.543	0.329	0.058	0.070	
		0.607	0.277	0.042	0.074	
		0.603	0.276	0.045	0.076	
		0.606	0.277	0.043	0.074	
		0.557	0.313	0.054	0.076	
		0.606	0.274	0.046	0.074	
PWR BWR LWGR GCR (Enriched Uranium)	f_i	0.488	0.359	0.067	0.087	Y. Abe et al. (2012)
		0.580	0.292	0.054	0.074	Z. Djurcic et al. (2009)
		0.544	0.318	0.063	0.075	
		0.577	0.292	0.057	0.074	
		0.590	0.290	0.050	0.070	V. I. Kopeikin et al. (2004)
		0.570	0.295	0.057	0.078	S. Abe et al. (2008)
		0.568	0.297	0.057	0.078	K. Eguchi et al. (2003)
		0.563	0.301	0.057	0.079	T. Araki et al. (2005)
		0.650	0.240	0.040	0.070	V. I. Kopeikin (2012)
		0.560	0.310	0.060	0.070	
		0.480	0.370	0.080	0.070	
	p_i	0.560	0.300	0.080	0.060	G. Bellini et al. (2010)
MOX	p_i	0.000	0.708	0.212	0.081	G. Bellini et al. (2010)
PHWR	p_i	0.543	0.411	0.022	0.024	G. Bellini et al. (2013)

Enriched Uranium

Mixed Oxide Fuel

Natural Uranium

Reactor antineutrino signal calculation

The reactor antineutrino signal evaluation requires several ingredients for modeling the three antineutrino life stages:

- ✓ **production** at reactor cores
- ✓ **propagation** to the detector site
- ✓ **detection** in liquid scintillation detectors

DETECTOR

- ε = 100% efficiency
- τ = 1 year
- $N_p = 10^{32}$ free protons (~ 1kton liquid scintillator mass)

ν PHYSICS

- P_{ee} = ν_e oscillation survival probability
- $\sigma_{IBD}(E)$ = IBD cross section

$\bar{\nu}_e + p \rightarrow e^+ + n$ (E_{th} = 1.806 MeV)

$$N_{TOT} = \varepsilon N_p \tau \sum_{k=1}^{N_{reactor}} \frac{P_{th}{}^{i}}{4\pi d_k^2} \langle LF_k \rangle \int dE_\nu \sum_{i=1}^{4} \frac{p_i}{Q_i} \lambda_i(E_\nu) P_{ee}(E_\nu, d_k) \sigma_{IBD}(E_\nu)$$

[1 TNU = 1 event / 10^{32} free protons /year]

$i = {}^{235}U, {}^{238}U, {}^{239}Pu, {}^{241}Pu$

REACTOR

- d_k = reactor distance
- P_k = thermal power
- LF = Load Factor
- p_k = power fraction

NUCLEAR

- Q_i = energy released per fission
- λ_i = reactor antineutrino spectrum

Reactor antineutrino signal calculation

The reactor antineutrino signal evaluation requires several ingredients for modeling the three antineutrino life stages:

- ✓ **production** at reactor cores
- ✓ **propagation** to the detector site
- ✓ **detection** in liquid scintillation detectors

DETECTOR

- ε = 100% efficiency
- τ = 1 year
- $N_p = 10^{32}$ free protons (~ 1kton liquid scintillator mass)

ν PHYSICS

- P_{ee} = ν_e oscillation survival probability
- $\sigma_{IBD}(E)$ = IBD cross section

$\bar{\nu}_e + p \rightarrow e^+ + n$ (E_{th} = 1.806 MeV)

$$N_{TOT} = \varepsilon N_p \tau \sum_{k=1}^{N_{reactor}} \frac{P_{th}{}^{i}}{4\pi d_k^2} \langle LF_k \rangle \int dE_\nu \sum_{i=1}^{4} \frac{p_i}{Q_i} \lambda_i(E_\nu) P_{ee}(E_\nu, d_k) \sigma_{IBD}(E_\nu)$$

[1 TNU = 1 event / 10^{32} free protons /year]

$i = {}^{235}U, {}^{238}U, {}^{239}Pu, {}^{241}Pu$

REACTOR

- d_k = reactor distance
- P_k = thermal power
- LF = Load Factor
- p_k = power fraction

NUCLEAR

- Q_i = energy released per fission
- λ_i = reactor antineutrino spectrum

Reactor and geoneutrino signals at 6 experimental sites

Experiment	G [TNU]	R_{LER} [TNU]	$r = R_{LER}/G$	Year
KamLAND	$31.5^{+4.9}_{-4.1}$	$168.5^{+5.7}_{-6.3}$	5.4	2006
		$18.3^{+0.6}_{-1.0}$	0.6	2013
		$7.4^{+0.2}_{-0.2}$	0.2	2014
JUNO	$39.7^{+6.5}_{-5.1}$	$26.0^{+2.2}_{-2.3}$	0.7	2013
		$53.9^{+3.0}_{-2.8}$	1.4	2014
		$354.5^{+44.5}_{-40.6}$	8.9	2020
Borexino	$40.3^{+7.3}_{-3.8}$	$22.2^{+0.6}_{-0.6}$	0.6	2013
SNO+	$45.4^{+7.5}_{-6.3}$	$47.8^{+1.7}_{-1.4}$	1.1	2013
RENO-50	$42.1^{+7.2}_{-5.9}$	$178.4^{+20.8}_{-19.6}$	4.2	2013
Hanohano	$12.0^{+0.7}_{-0.6}$	$0.9^{+0.02}_{-0.02}$	0.1	2013

Ohi 3 and Ohi 4 powered off

Yangjiang and Taishan fully powered on in 2020

Long Baseline experiments: 1σ ~ 4% in LER

Signal uncertainty due to individual inputs

Input quantity		*1σ on signal in FER [%]* Borexino	KamLAND	SNO+
ν oscillation	δm^2 (eV)^2	<0.1	0.9	<0.1
	$sen^2\theta_{12}$	+2.4/-2.2	+2.1/-2.0	+2.4/-2.2
	$sen^2\theta_{13}$	0.4	0.4	0.4
Energy per fission	Q_{235U}	<0.1	<0.1	<0.1
	Q_{238U}			
	Q_{239Pu}			
	Q_{241Pu}			
Fission fraction	f_{235U}	0.1	0.5	<0.1
	f_{238U}			
	f_{239Pu}			
	f_{241Pu}			
Thermal Power	P_{th}	0.2	0.9	0.3
IBD cross section	σ_{IBD}	<0.1	<0.1	<0.1

- ✓ Reactor signal uncertainty **dominated by $sin^2(\vartheta_{12})$**
- ✓ Results are **time dependent** (2013 status) and **site dependent**
- ✓ Signal uncertainty due to P_{th} reflects the **signal amount generated by single reactors** (for KamLAND 60% of the signal originated by 2 cores)
- ✓ **Negligible** (<0.1%) uncertainty from Q_i and σ_{IBD}

Borexino, KamLAND and SNO+ signal distance profile

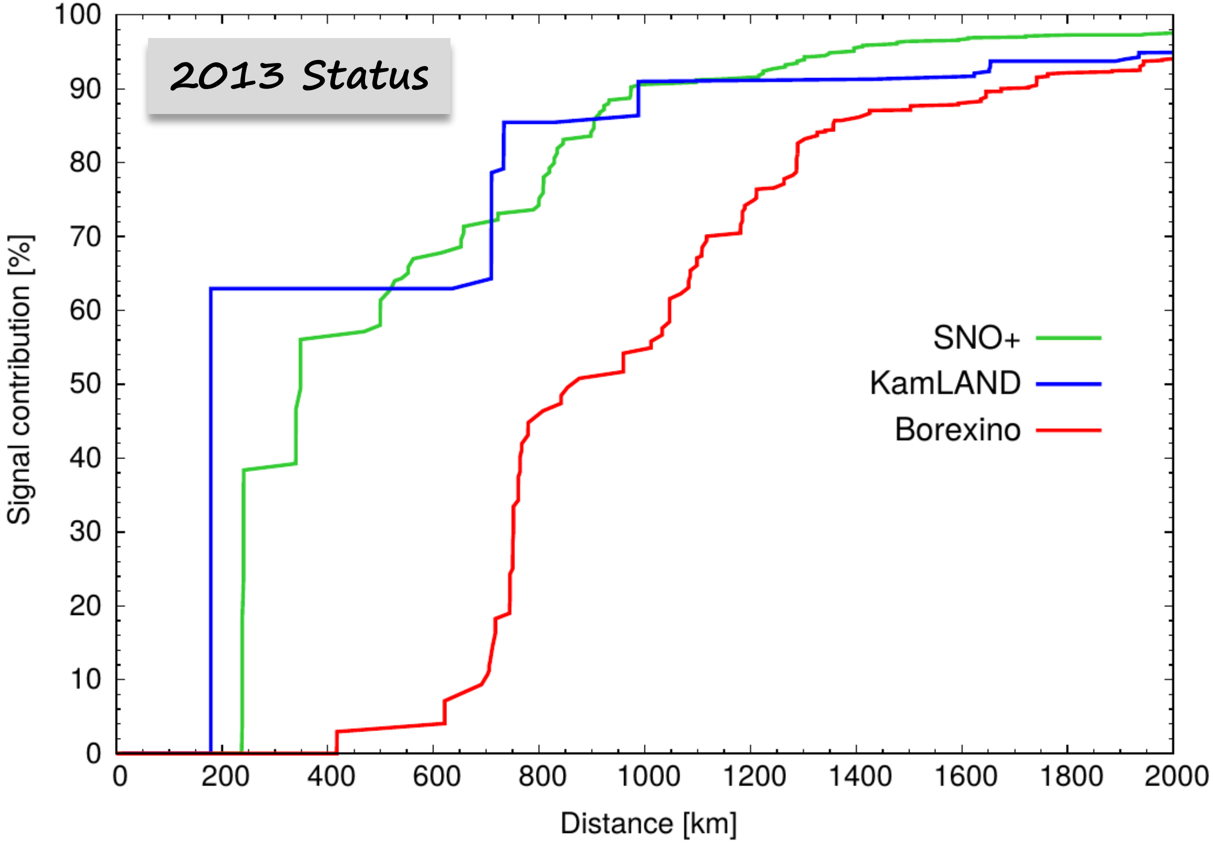

KL step-like profile with **3 major discontinuities**

- ✓ **1st** is **~60%** at **180 km** (Japanese Ohi3 and Ohi4)
- ✓ **2nd** is **~85%** at **730 km** (Japanese plus East coast South Korean)
- ✓ **3rd** is **~90%** at **990 km** (Japanese plus all South Korean)

SNO+ profile has **2 major discontinuities**

- ✓ **1st** is **~38%** at **~240 km** (Canadian Bruce)
- ✓ **2nd** is **~56%** at **~350 km** (Canadian Pickering and Darlington)
- ✓ For **d > 500km** the profile **levels out** (USA stations)

BX profile is **smooth**

- ✓ Signal **spread out** over the European countries
- ✓ Closest power station at **415 km** (Slovenia) gives the major fraction of the signal (**~3%**)

Borexino and KamLAND signal time profile

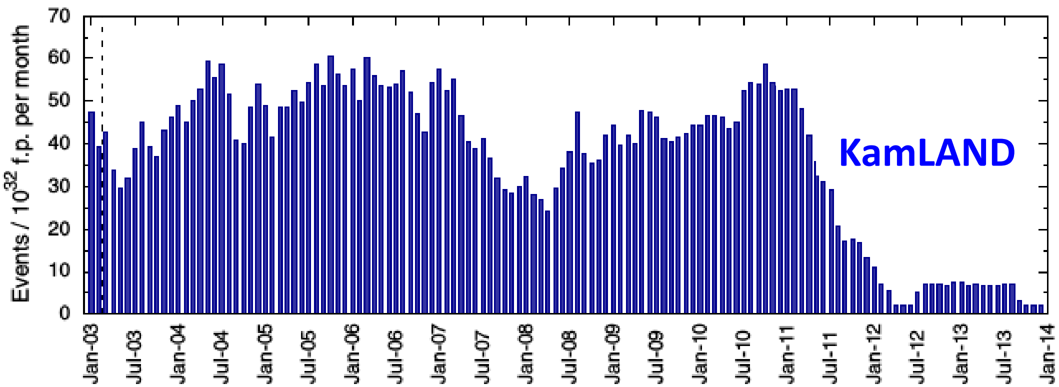

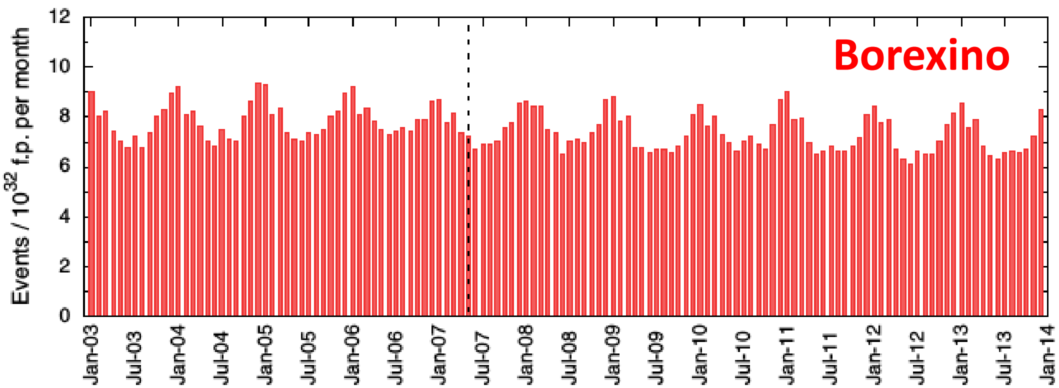

- ✓**Seasonal signal variation** associated with the lower fall-spring electricity demand
- ✓Relatively **insensitive** to **operational conditions** of **single reactors** since there are no close-by reactors dominating the antineutrino flux

- ✓Signal time profile governed by the **Japanese nuclear industry** operational status
- ✓Shutdown of nuclear power plants concomitant to strong **earthquakes** manifestly visible
- ✓**Sensitive** to **operational conditions** of **single reactors**

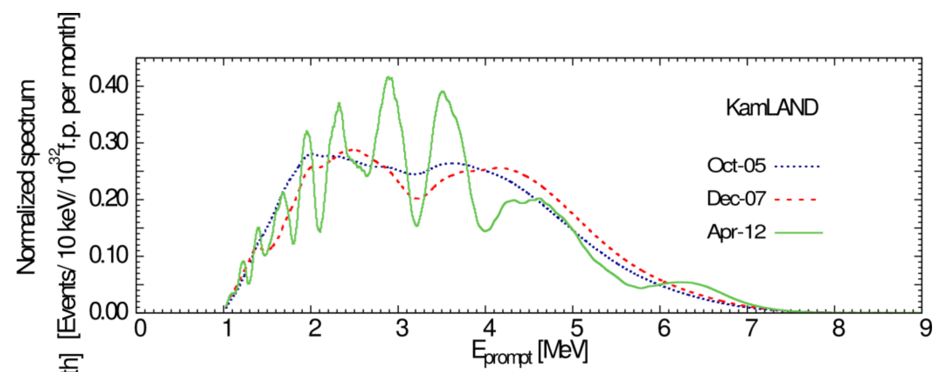

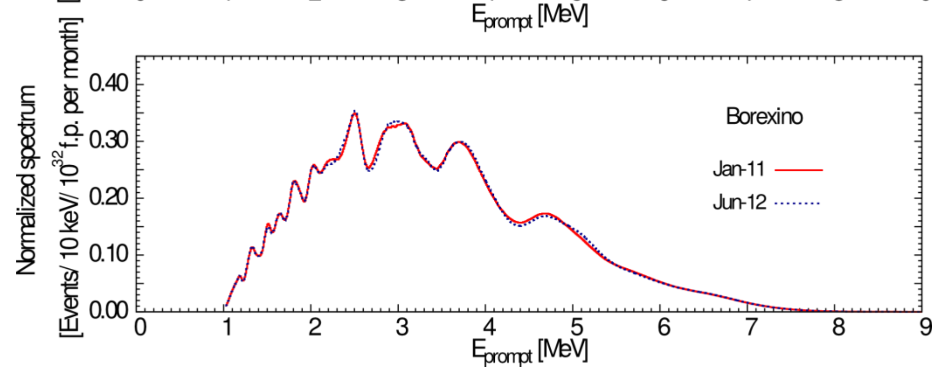

Borexino and KamLAND signal time profile

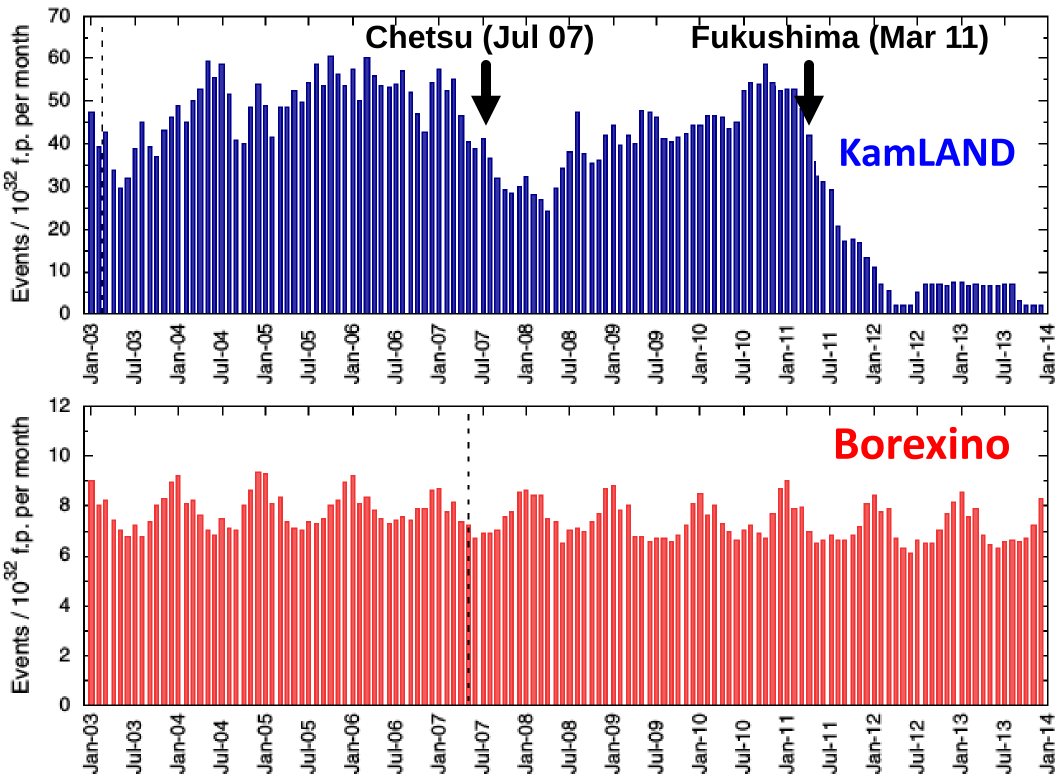

- ✓ Signal time profile governed by the **Japanese nuclear industry** operational status
- ✓ Shutdown of nuclear power plants concomitant to strong **earthquakes** manifestly visible
- ✓ **Sensitive** to **operational conditions** of **single reactors**

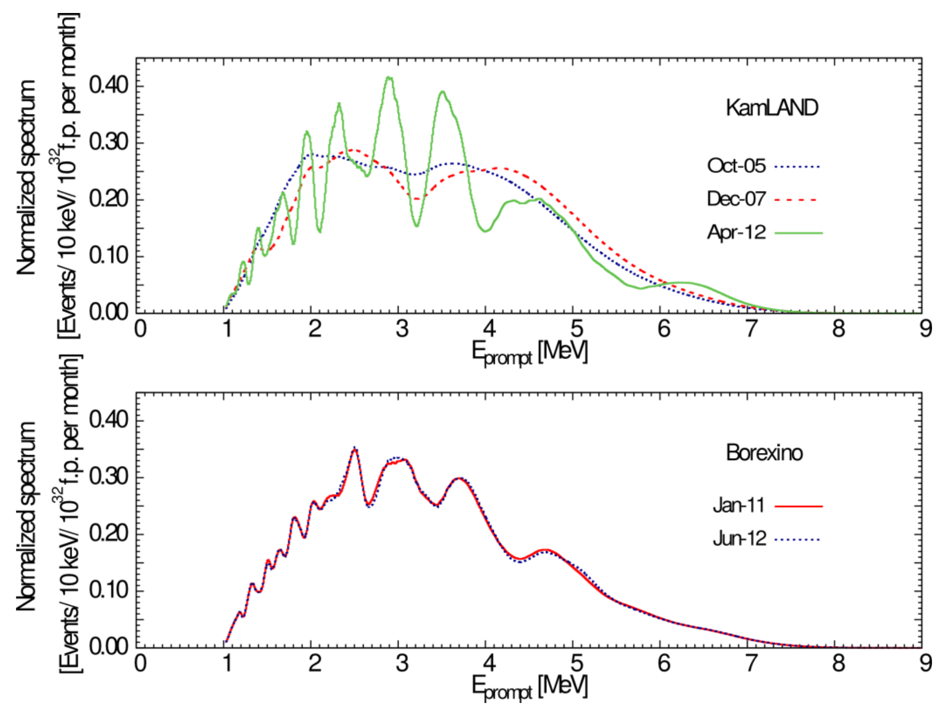

- ✓ **Seasonal signal variation** associated with the lower fall-spring electricity demand
- ✓ Relatively **insensitive** to **operational conditions** of **single reactors** since there are no close-by reactors dominating the antineutrino flux

Borexino and KamLAND signal time profile

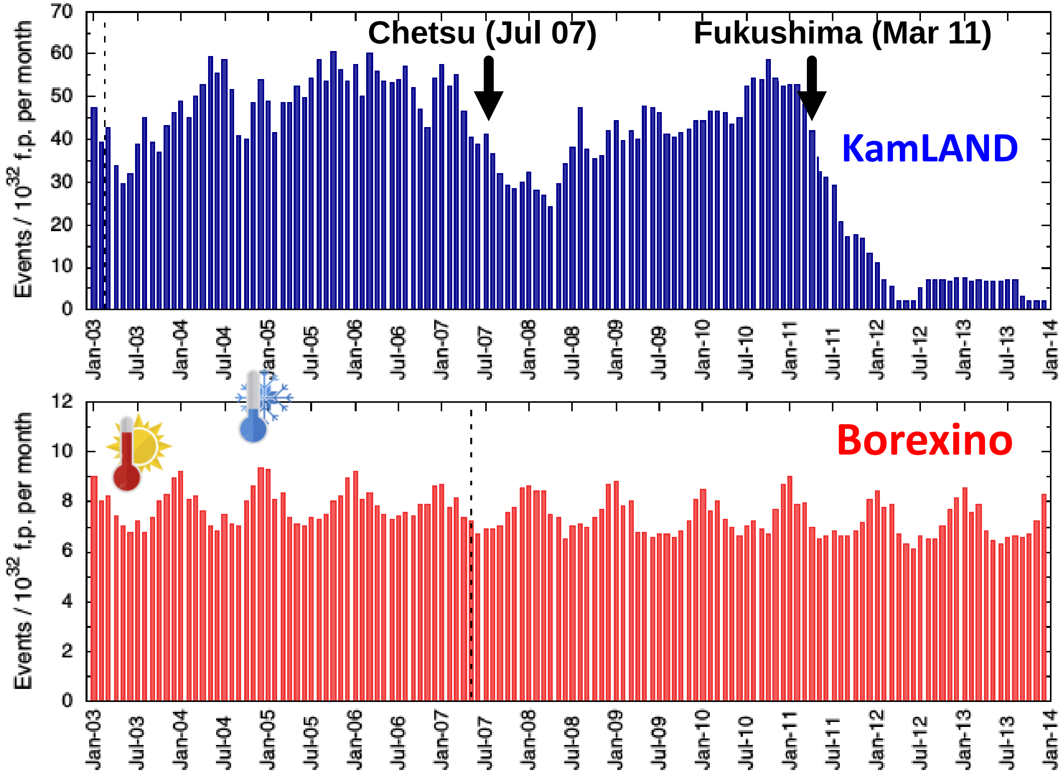

✓Signal time profile governed by the **Japanese nuclear industry** operational status

✓Shutdown of nuclear power plants concomitant to strong **earthquakes** manifestly visible

✓**Sensitive** to **operational conditions** of **single reactors**

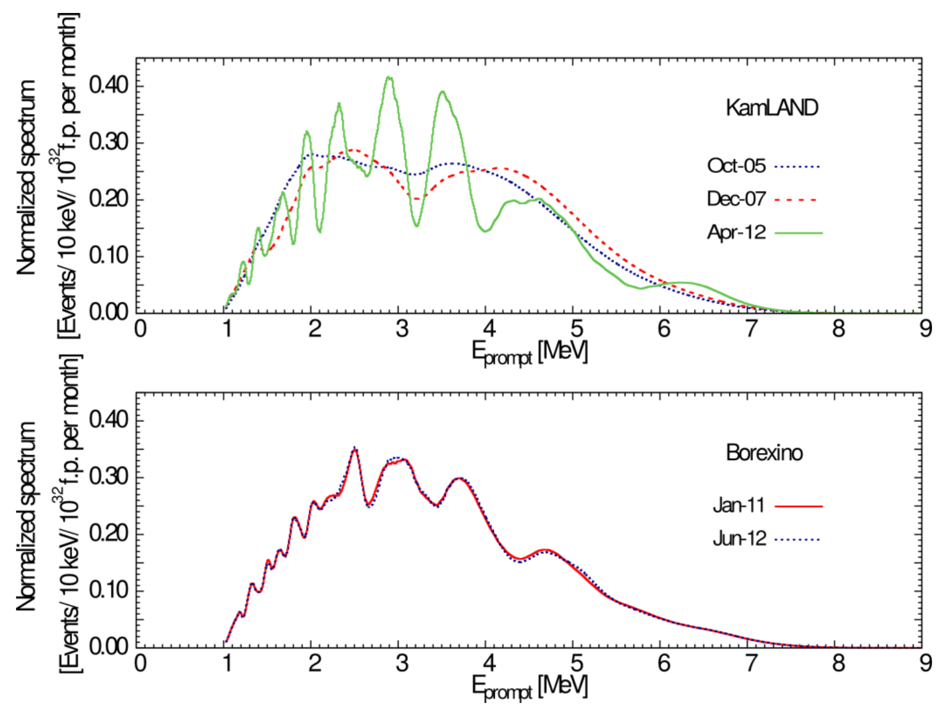

✓**Seasonal signal variation** associated with the lower fall-spring electricity demand

✓Relatively **insensitive** to **operational conditions** of **single reactors** since there are no close-by reactors dominating the antineutrino flux

Outcomes of this work

The web page **www.fe.infn.it/antineutrino** provides an **updated collection** of data about worldwide nuclear reactors for calculation of antineutrino signal

2003

- Input database
- Numerical map
- Map

2004

- Input database
- Numerical map
- Map

2005

- Input database
- Numerical map
- Map

2006

- Input database
- Numerical map
- Map

2007

- Input database
- Numerical map
- Map

2008

- Input database
- Numerical map
- Map

2009

- Input database
- Numerical map
- Map

2010

- Input database
- Numerical map
- Map

2011

- Input database
- Numerical map
- Map

2012

- Input database
- Numerical map
- Map

2013

- Input database
- Numerical map
- Map

2014

- Input database
- Numerical map
- Map

2015

- Input database
- Numerical map
- Map

Outcomes of this work

The web page **www.fe.infn.it/antineutrino** provides an **updated collection** of data about worldwide nuclear reactors for calculation of antineutrino signal

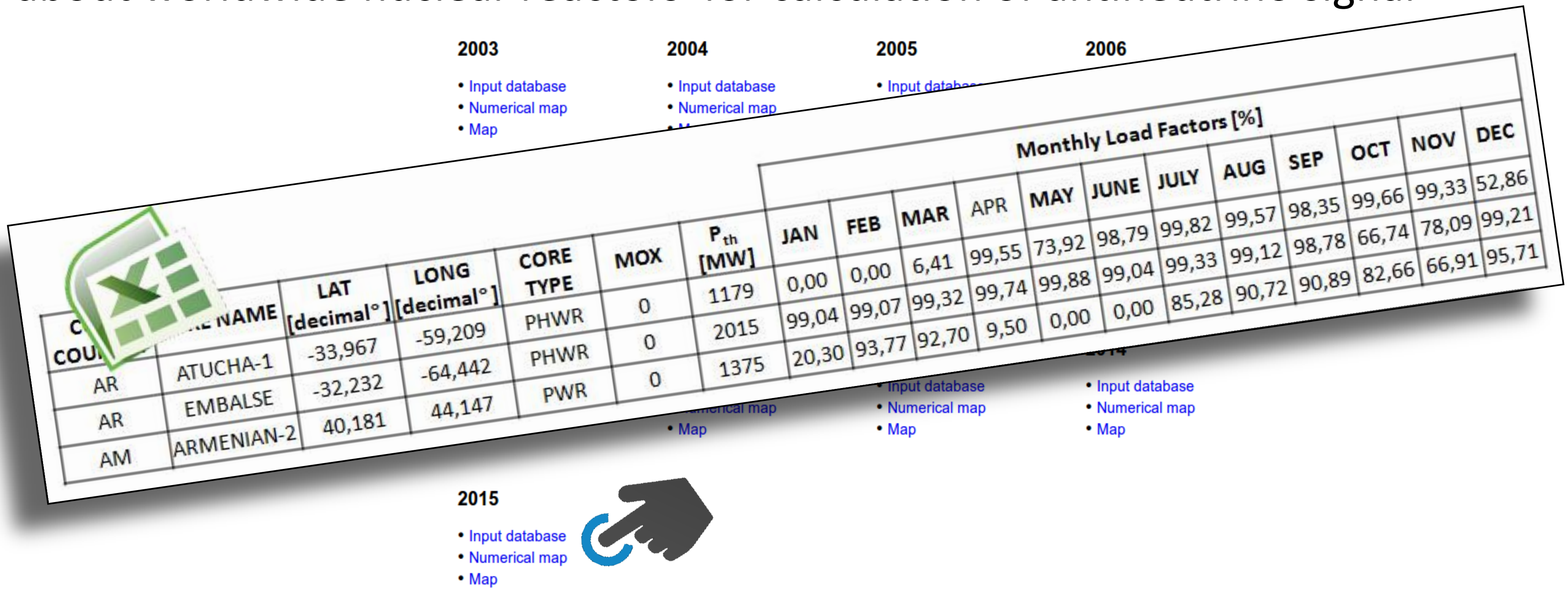

COU	NAME	LAT [decimal°]	LONG [decimal°]	CORE TYPE	MOX	P_{th} [MW]	Monthly Load Factors [%]											
							JAN	FEB	MAR	APR	MAY	JUNE	JULY	AUG	SEP	OCT	NOV	DEC
AR	ATUCHA-1	-33,967	-59,209	PHWR	0	1179	0,00	0,00	6,41	99,55	73,92	98,79	99,82	99,57	98,35	99,66	99,33	52,86
AR	EMBALSE	-32,232	-64,442	PHWR	0	2015	99,04	99,07	99,32	99,74	99,88	99,04	99,33	99,12	98,78	66,74	78,09	99,21
AM	ARMENIAN-2	40,181	44,147	PWR	0	1375	20,30	93,77	92,70	9,50	0,00	0,00	85,28	90,72	90,89	82,66	66,91	95,71

- ✓ **Global**: performance data of **all reactors in the world**
- ✓ **Monthly Load Factors** (%)
- ✓ **Public, official** and **free**
- ✓ **Latitude** and **longitude** of reactors
- ✓ **Multitemporal**: time lapse of **12 years** (2003 – 2015)
- ✓ **Direct implementation** thanks to standard file

Outcomes of this work

The web page **www.fe.infn.it/antineutrino** provides an **updated collection** of data about worldwide nuclear reactors for calculation of antineutrino signal

2003
- Input database
- Numerical map
- Map

2004
- Input database
- Numerical map

2005

2006

C COU	NAME	LAT [decimal°]	LONG [decimal°]	CORE TYPE	MOX	P_{th} [MW]	Monthly Load Factors [%] JAN	FEB	MAR	APR	MAY	JUNE	JULY	AUG	SEP	OCT	NOV	DEC
AR	ATUCHA-1	-33,967	-59,209	PHWR	0	1179	0,00	0,00	6,41	99,55	73,92	98,79	99,82	99,57	98,35	99,66	99,33	52,86
AR	EMBALSE	-32,232	-64,442	PHWR	0	2015	99,04	99,07	99,32	99,74	99,88	99,04	99,33	99,12	98,78	66,74	78,09	99,21
AM	ARMENIAN-2	40,181	44,147	PWR	0	1375	20,30	93,77	92,70	9,50	0,00	0,00	85,28	90,72	90,89	82,66	66,91	95,71

- Input database
- Numerical map
- Map

2014
- Input database
- Numerical map
- Map

2015
- Input database
- Numerical map
- Map

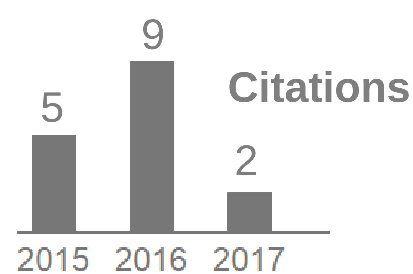

- ✓ **Global**: performance data of **all reactors in the world**
- ✓ **Monthly Load Factors** (%)
- ✓ **Public, official** and **free**
- ✓ **Latitude** and **longitude** of reactors
- ✓ **Multitemporal**: time lapse of **12 years** (2003 – 2015)
- ✓ **Direct implementation** thanks to standard file

Baldoncini M., et al. - *Reference worldwide model for antineutrinos from reactors.* **Phys. Rev. D** 91, 065002, (2015).


New challenges in...
...the spectral reconstruction of...
...terrestrial gamma rays and...
...reactor antineutrinos

Gamma-ray spectroscopy for studying the Earth

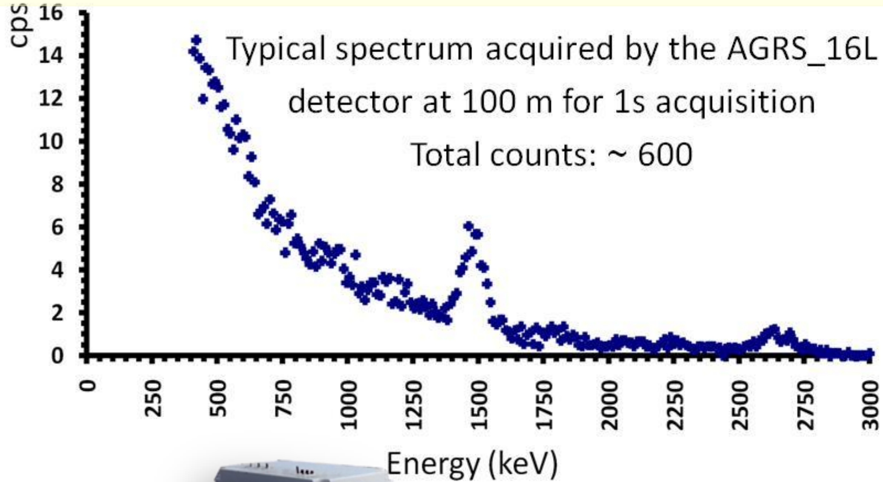

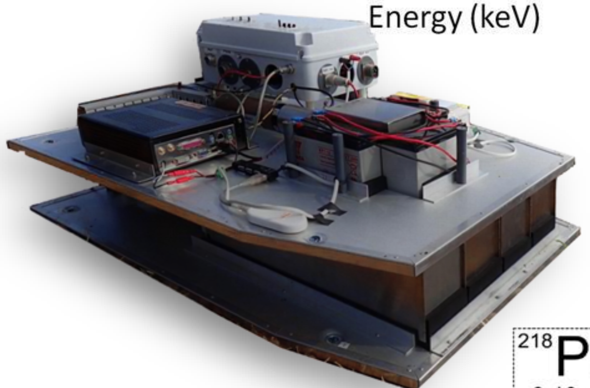

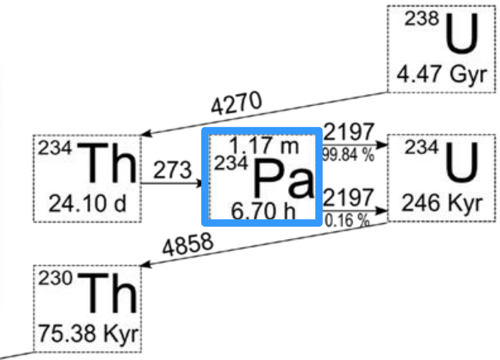

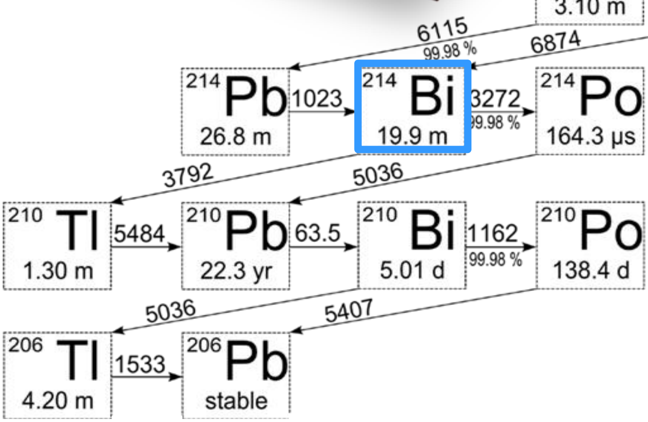

Isotope	Daughter	Energy (keV)	Half life	Typical abund.
^{40}K	/	1460	1.3 Gy	2%
^{238}U	^{234}Pa, ^{214}Bi	609, 1120, 1765	4.5 Gy	3 μg/g
^{232}Th	^{228}Ac, ^{208}Tl	911, 2614	14.1 Gy	10 μg/g

Calibrating an Airborne Gamma-Ray Spectrometer

GOAL: understand the **detector response function** to a known radioactive source

$$N = C \cdot FS$$

Measurement of **gamma spectra** at natural calibration sites

HPGe measurement of radioactive content on collected samples

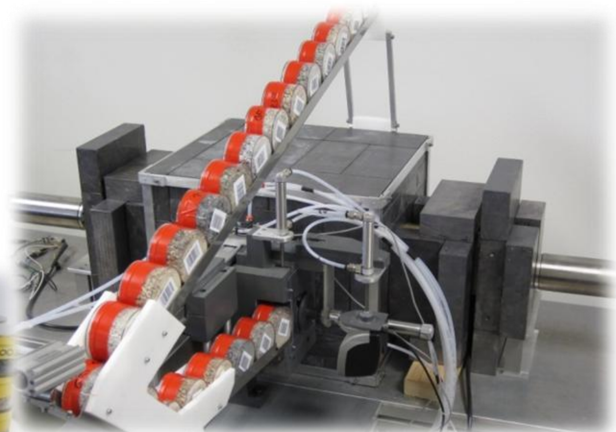

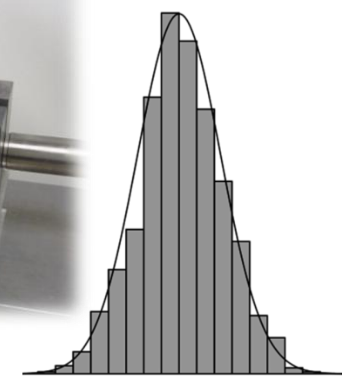

Modeling the calibration sites

Calibrating an Airborne Gamma-Ray Spectrometer

GOAL: understand the **detector response function** to a known radioactive source

Measurement of **gamma spectra** at natural calibration sites

$$N = C \cdot FS$$

Experimental Fundamental Spectra (EFS)

Monte Carlo Fundamental Spectra (MCFS)

HPGe measurement of radioactive content on collected samples

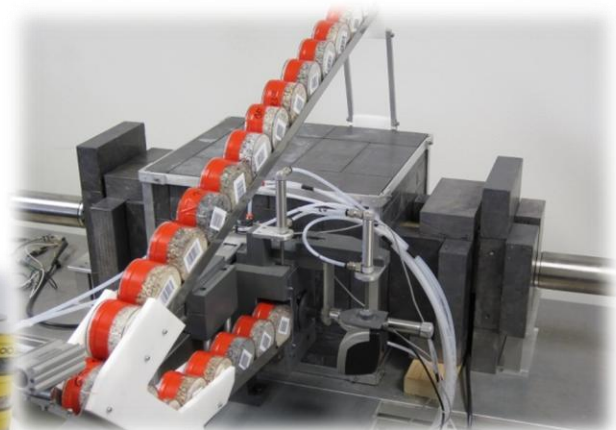

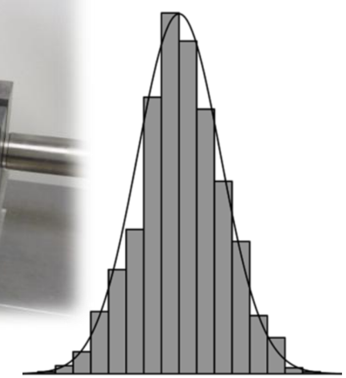

Modeling the calibration sites

Monte Carlo simulation strategy

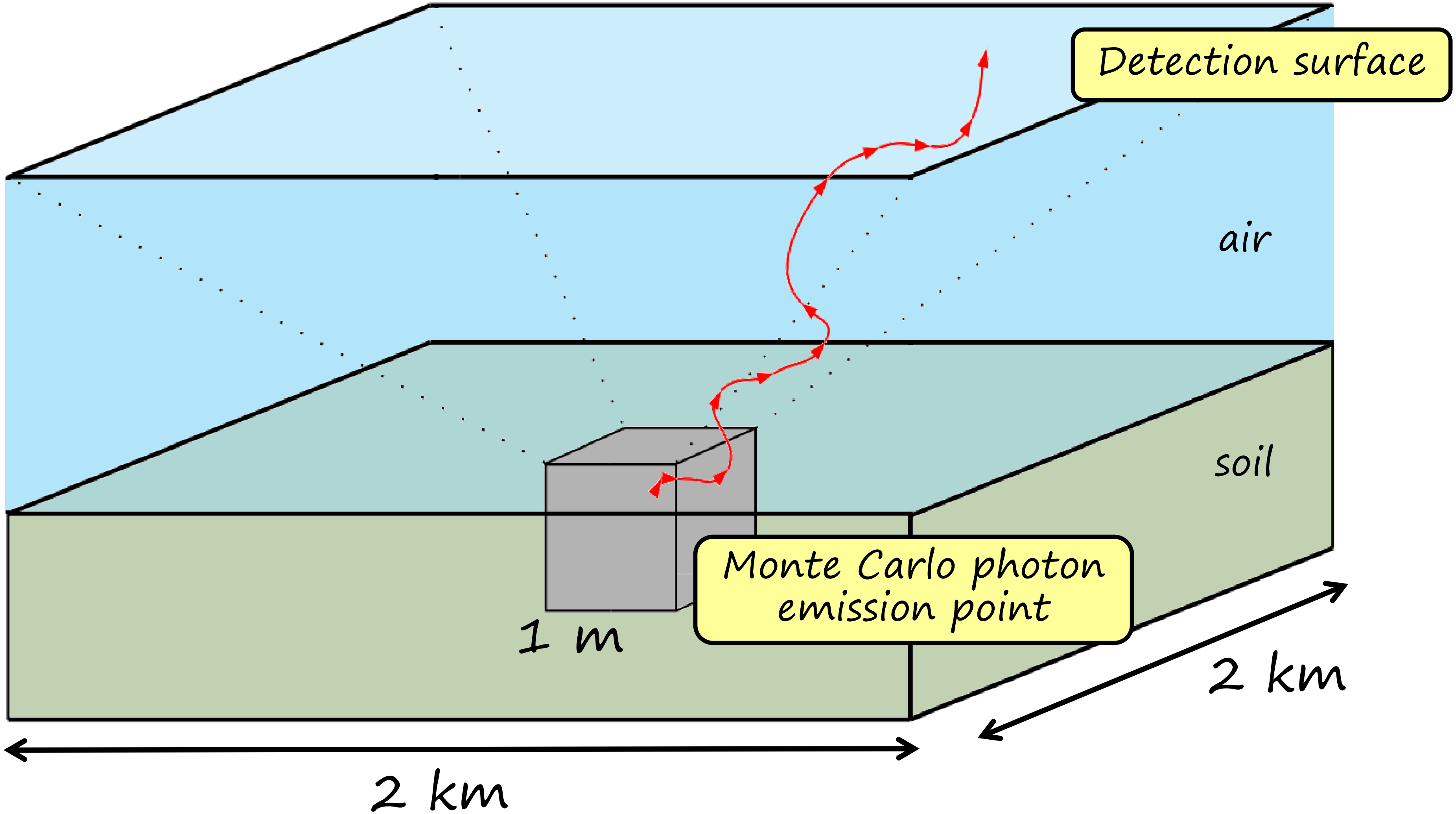

Monte Carlo simulation strategy

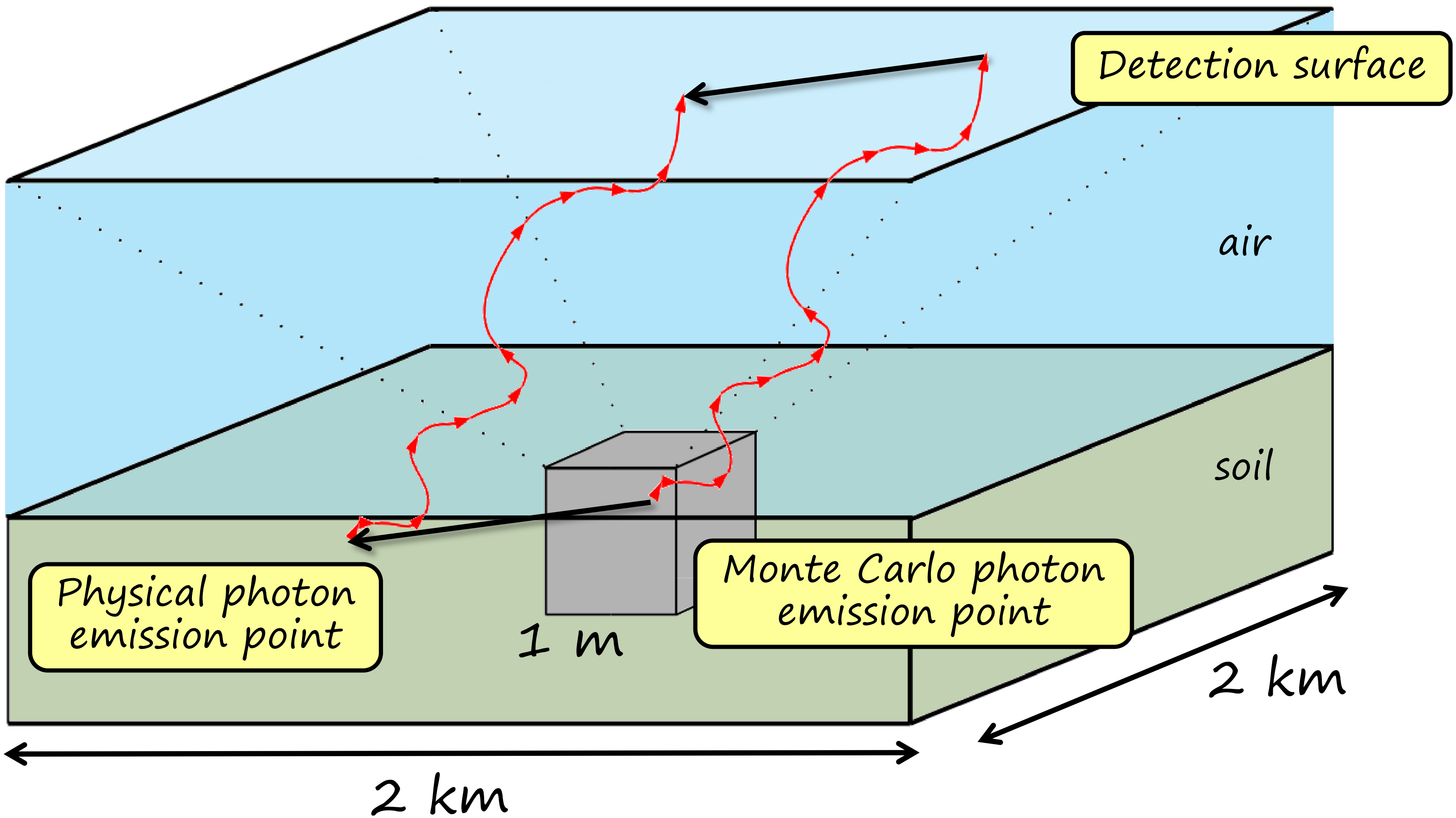

Monte Carlo simulation strategy

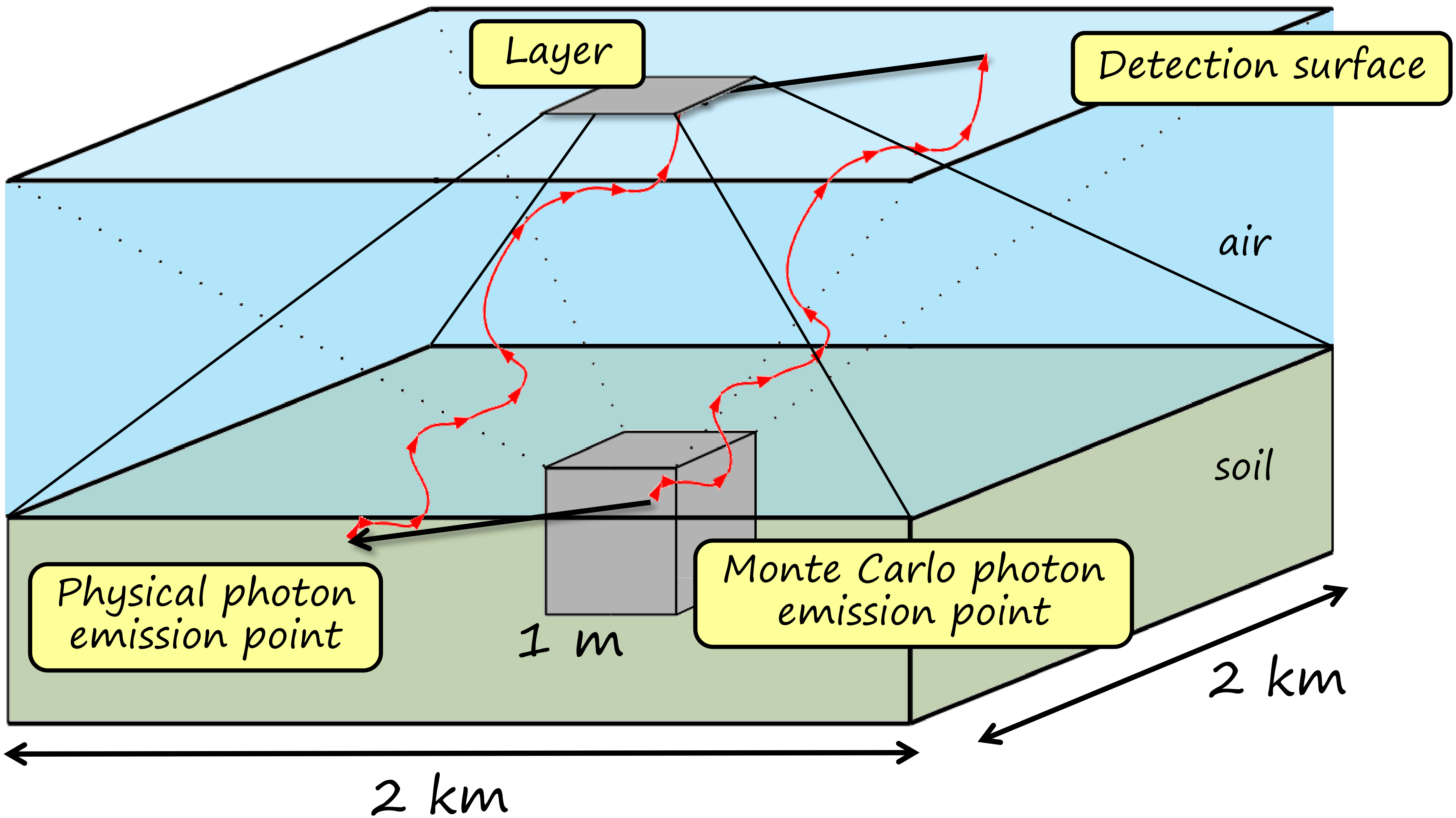

A shift of the photon arrival position is equivalent to a
shift of the photon emission point, without changing photon track.

Construction of Monte Carlo Fundamental Spectra

The detector is **sandwiched** between the layers of upward and downward moving photons

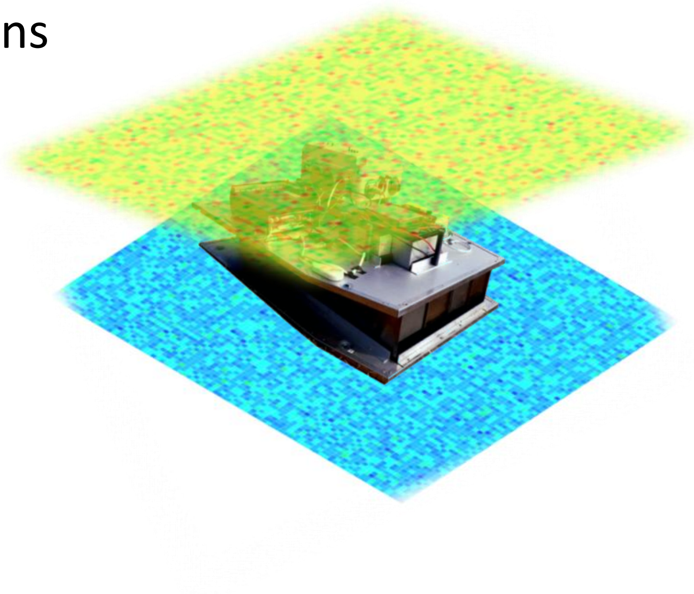

Construction of Monte Carlo Fundamental Spectra

The detector is **sandwiched** between the layers of upward and downward moving photons

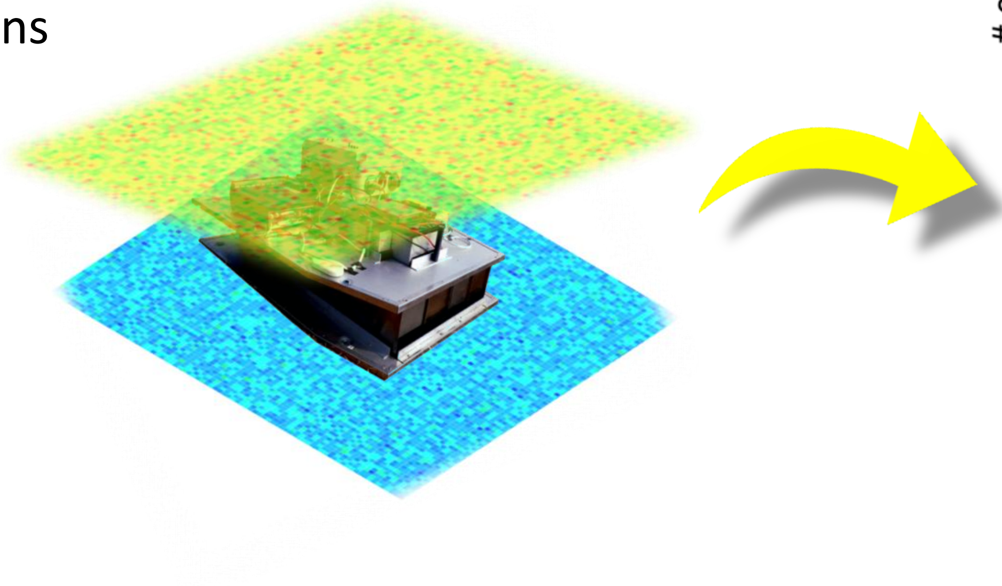

The Monte Carlo detector has **infinite energy resolution**

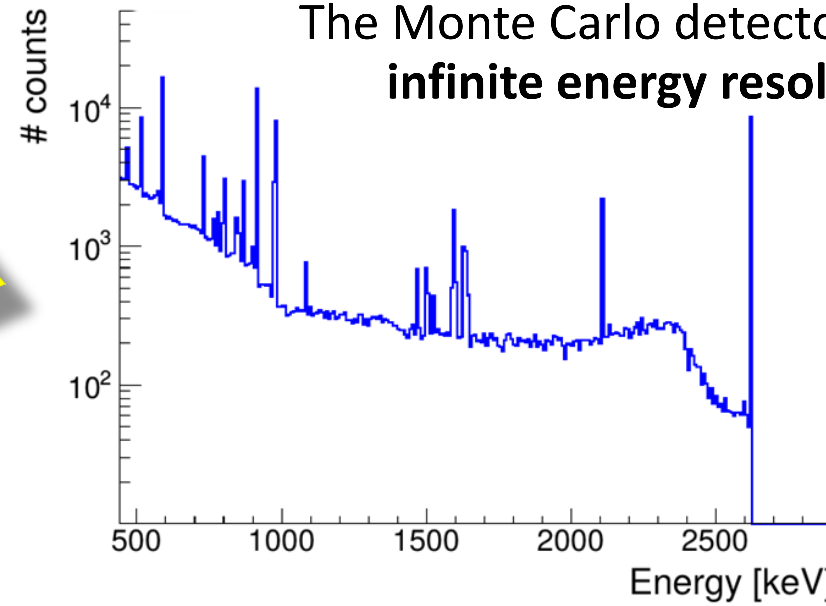

Construction of Monte Carlo Fundamental Spectra

The detector is **sandwiched** between the layers of upward and downward moving photons

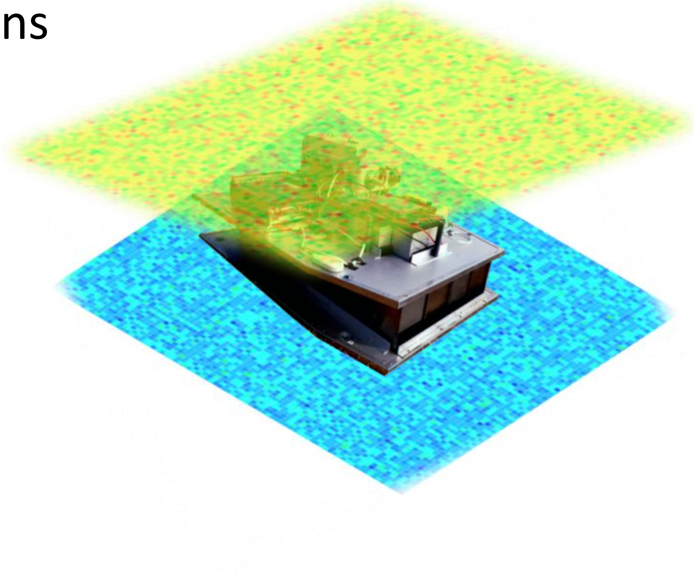

The Monte Carlo detector has **infinite energy resolution**

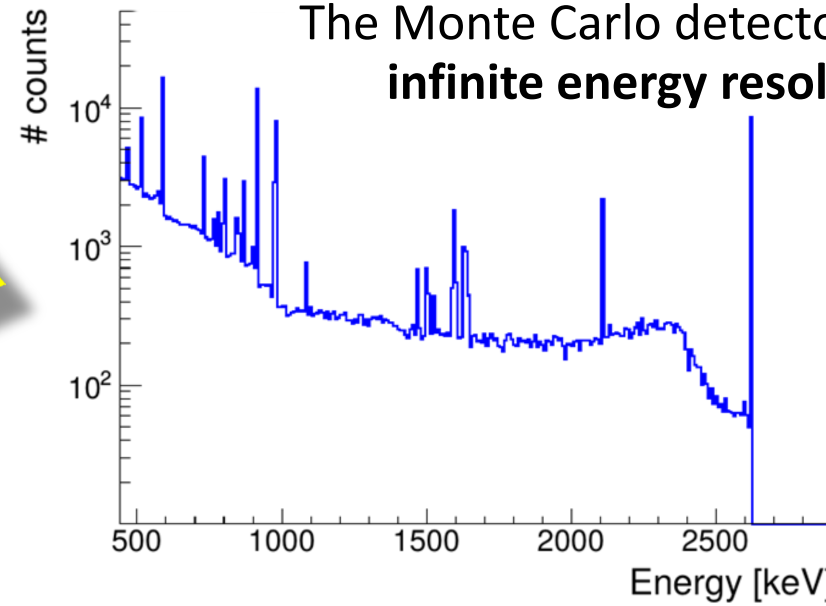

Experimental energy resolution for each detector

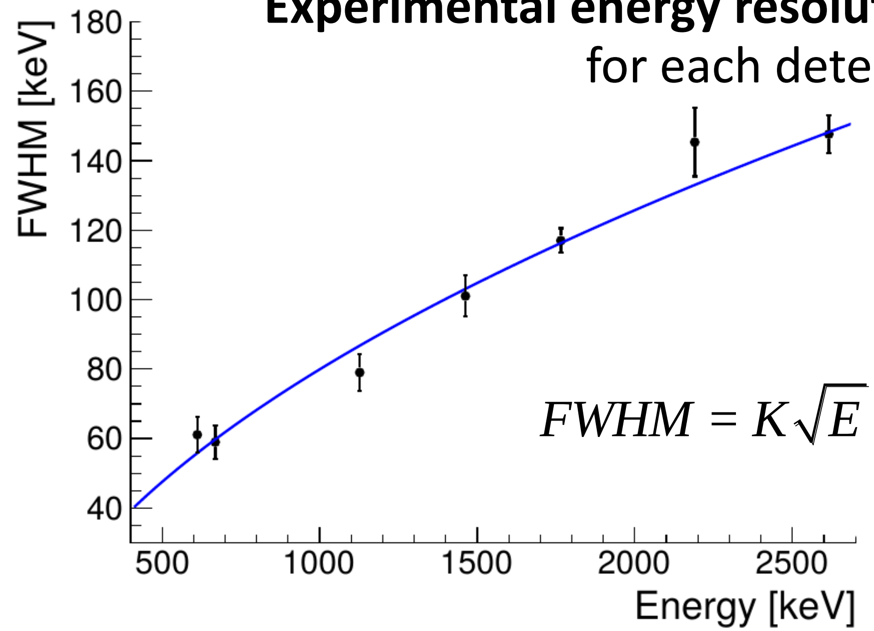

Construction of Monte Carlo Fundamental Spectra

The detector is **sandwiched** between the layers of upward and downward moving photons

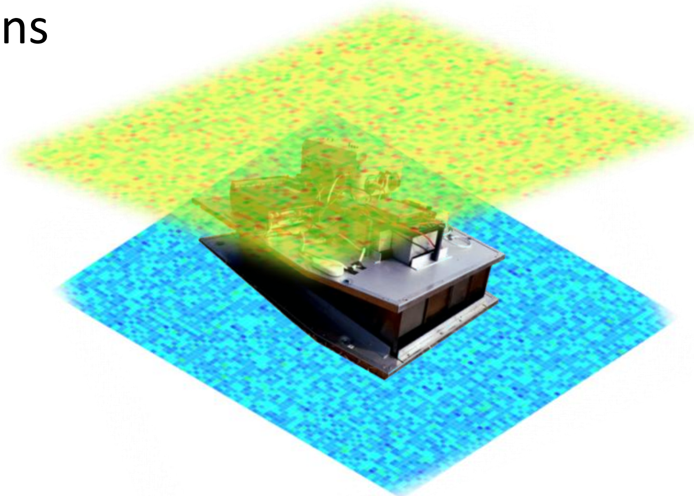

The Monte Carlo detector has **infinite energy resolution**

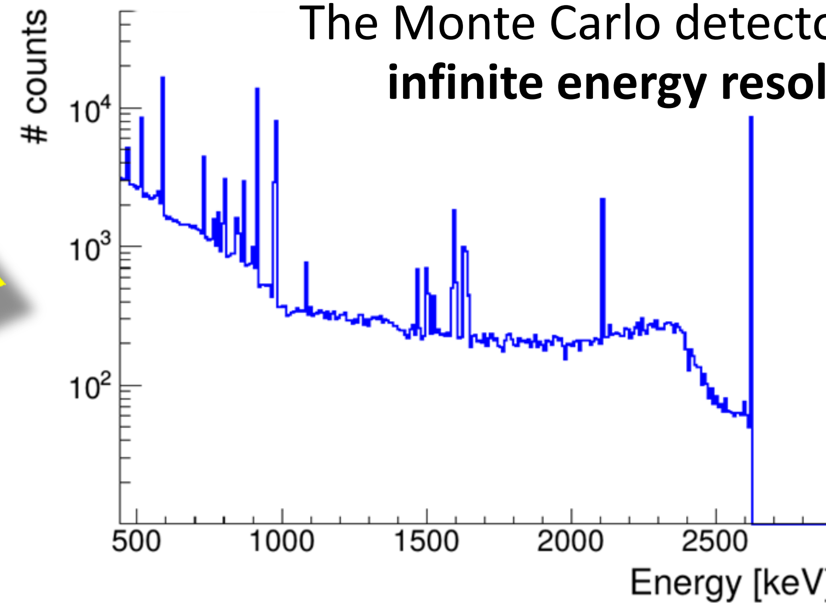

Experimental energy resolution for each detector

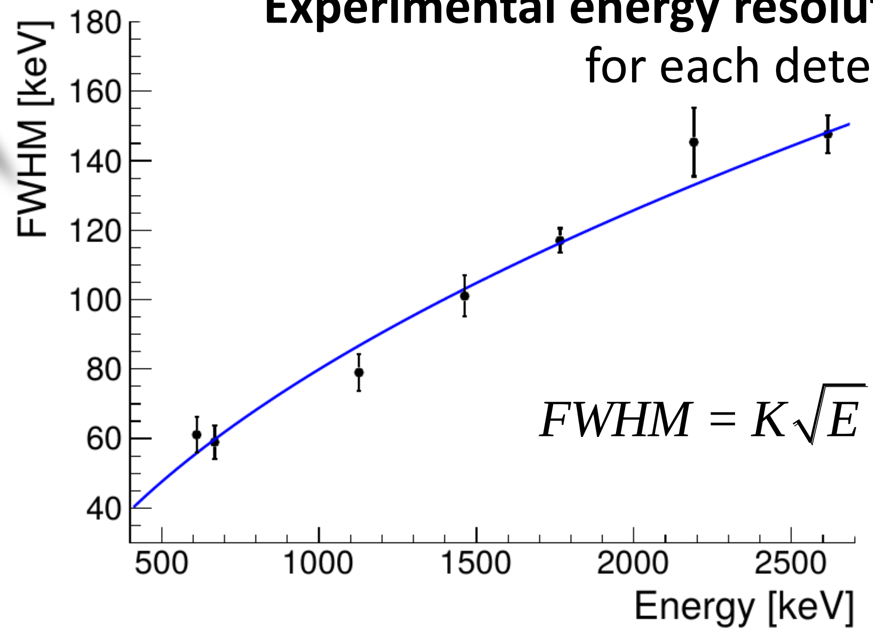

Monte Carlo spectrum

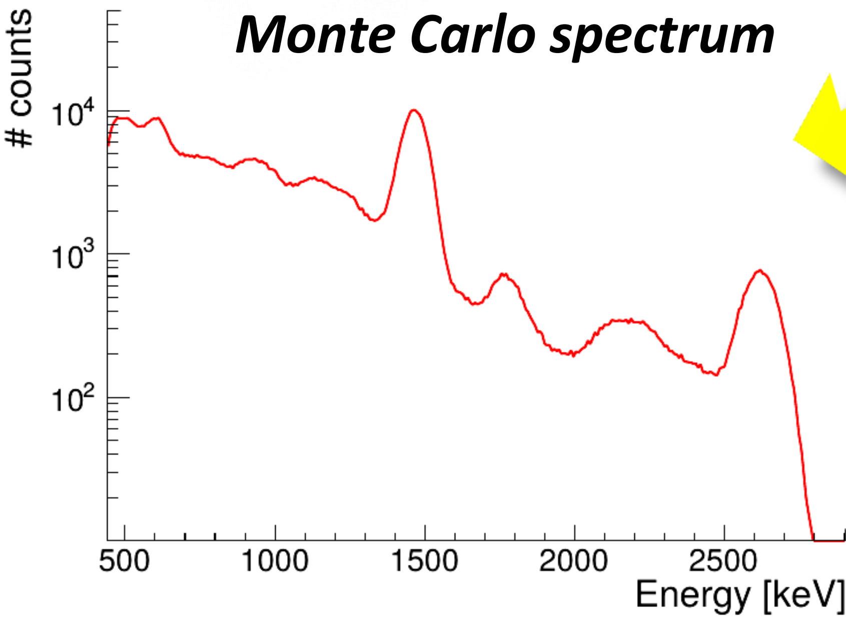

Experimental and Monte Carlo Fundamental Spectra

Experimental Fundamental Spectra

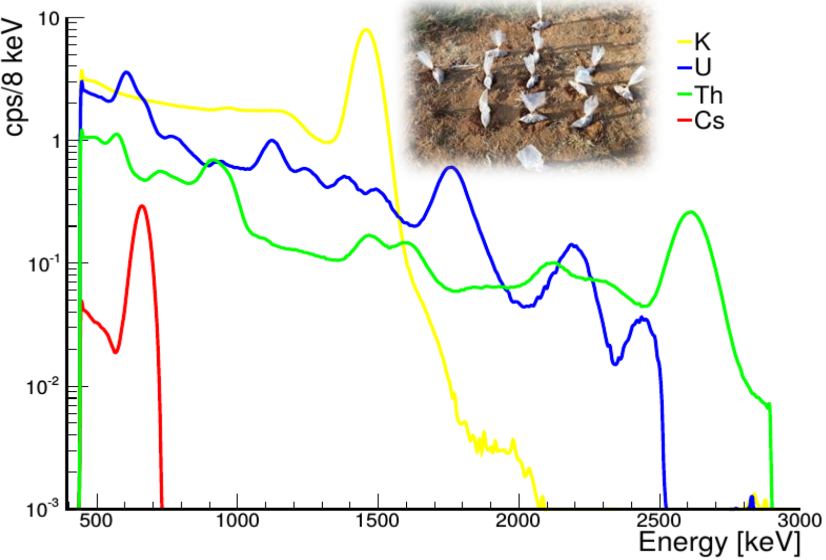

Monte Carlo Fundamental Spectra

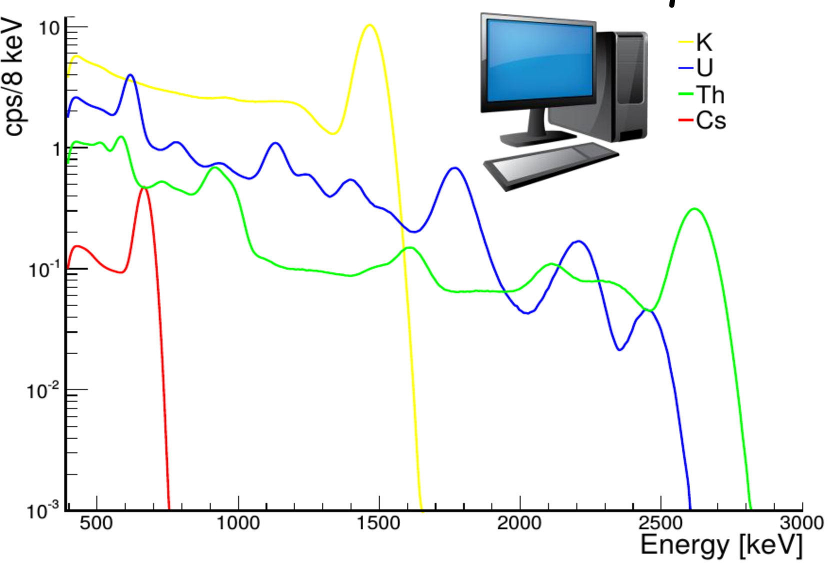

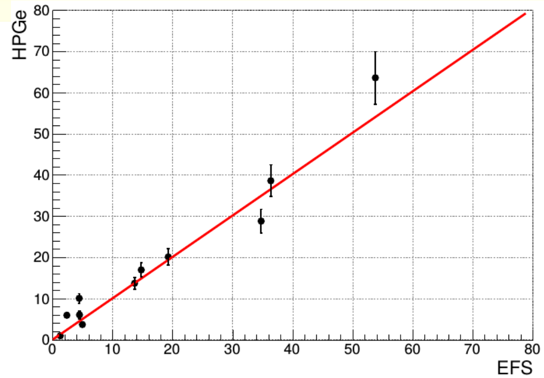

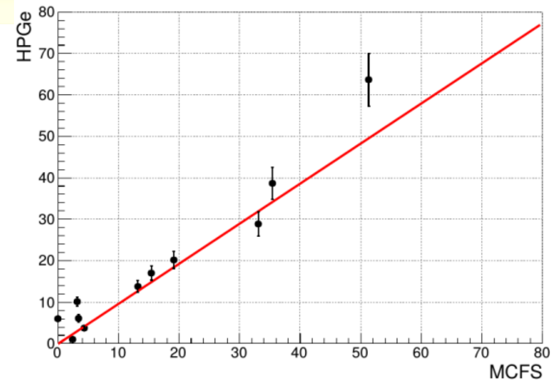

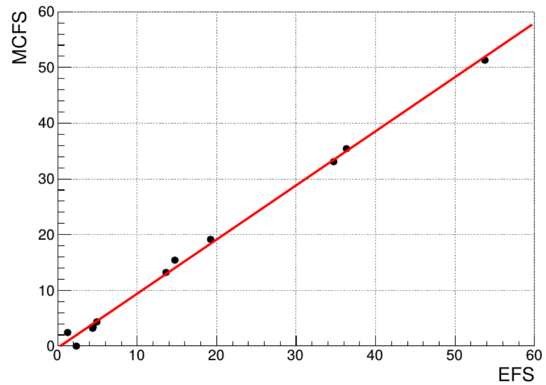

	$m \pm \delta m$	$q \pm \delta q$ ($\mu g/g$)	r^2
HPGe Vs EFS	1.01±0.04	0.10±0.22	0.956
HPGe Vs MCFS	0.97±0.05	-0.10±0.23	0.945
MCFS Vs EFS	0.97±0.02	-0.32±0.47	0.996

- ✓ EFS obtained by **modeling** the calibration sites
- ✓ **Redundancy** is the key and the tricky point of EFS extraction
- ✓ MCFS evaluated from an **ab-initio** approach
- ✓ Good **agreement** between **independent methods**
- ✓ EFS and MCFS highlight the **challenging** aspects in the efficiency calibration procedure (e.g. variability, field of view…)

Outcomes and perspectives of this study

- ✓ **Validation** of the **Monte Carlo** method for the AGRS_16L efficiency calibration
- ✓ For the first time we have **3 cards** to play: **Window Analysis Method**, **FSA-EFS** and **FSA-MCFS**
- ✓ **Monte Carlo** simulation solves the problem of providing the **detector response function** to **anthropic radionuclides** (e.g. ^{137}Cs fallout)
- ✓ **New detection systems** (e.g. UAV, mosaic detectors) characterized by different performances are entering the business of homeland security

Outcomes and perspectives of this study

- ✓ **Validation** of the **Monte Carlo** method for the AGRS_16L efficiency calibration
- ✓ For the first time we have **3 cards** to play: **Window Analysis Method**, **FSA-EFS** and **FSA-MCFS**
- ✓ **Monte Carlo** simulation solves the problem of providing the **detector response function** to **anthropic radionuclides** (e.g. ^{137}Cs fallout)
- ✓ **New detection systems** (e.g. UAV, mosaic detectors) characterized by different performances are entering the business of homeland security

Caciolli, A., **Baldoncini, M.**, et al., A new FSA approach for in situ γ ray spectroscopy. Science of The Total Environment.

Invitation to international AGC (**Aero Gamma Spectrometry Campaign**) in June 2017 in Zurich

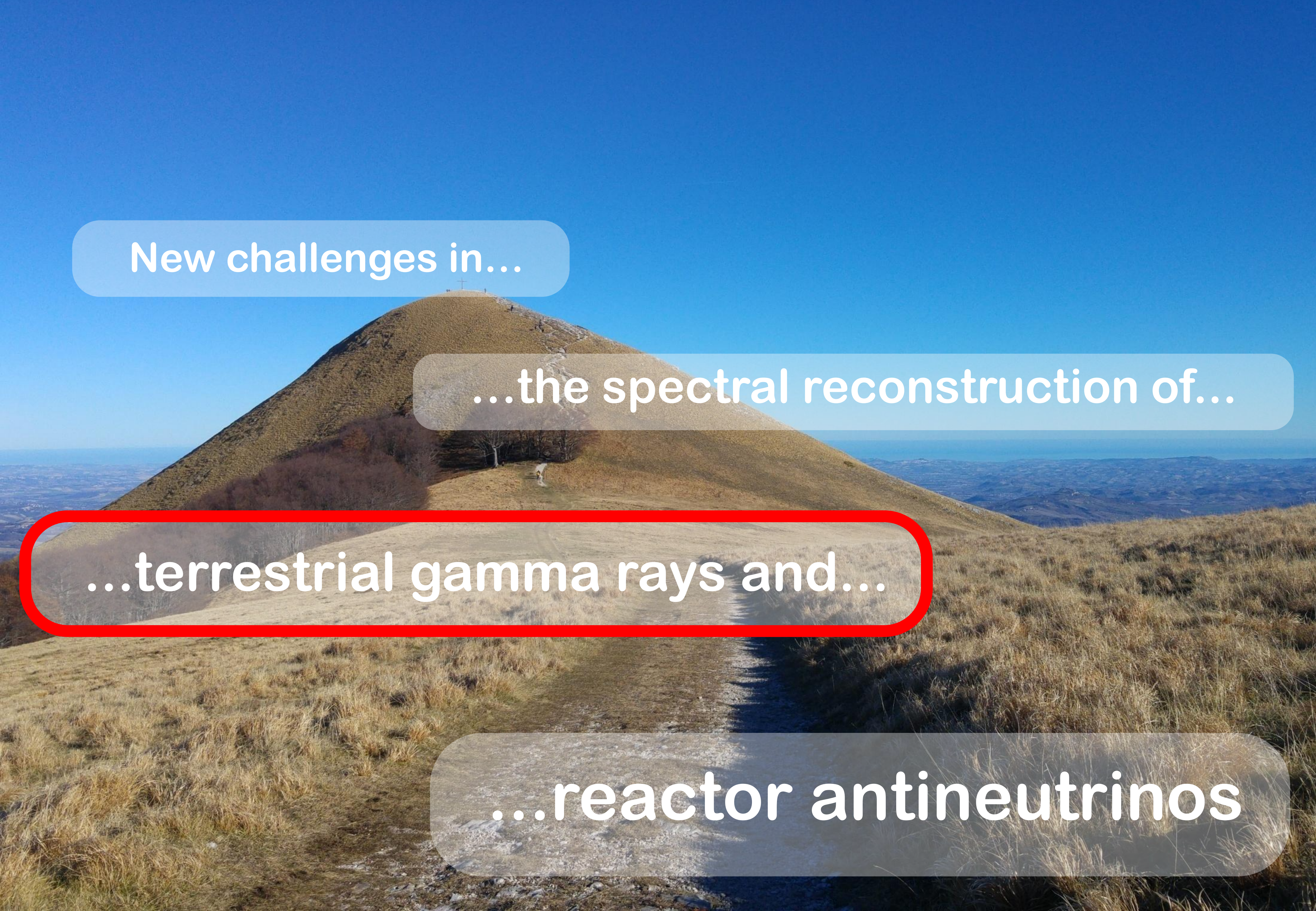
New challenges in...
...the spectral reconstruction of...
...terrestrial gamma rays and...
...reactor antineutrinos

Offshore background calibration flights for AGRS

GOAL: understand **background** radiation

- ✓ cosmic radiation due to the interaction of secondaries with the air and equipment
- ✓ **aircraft radiation** due to K, U and Th in the equipment
- ✓ **atmospheric radon** exhaled from rocks and soils

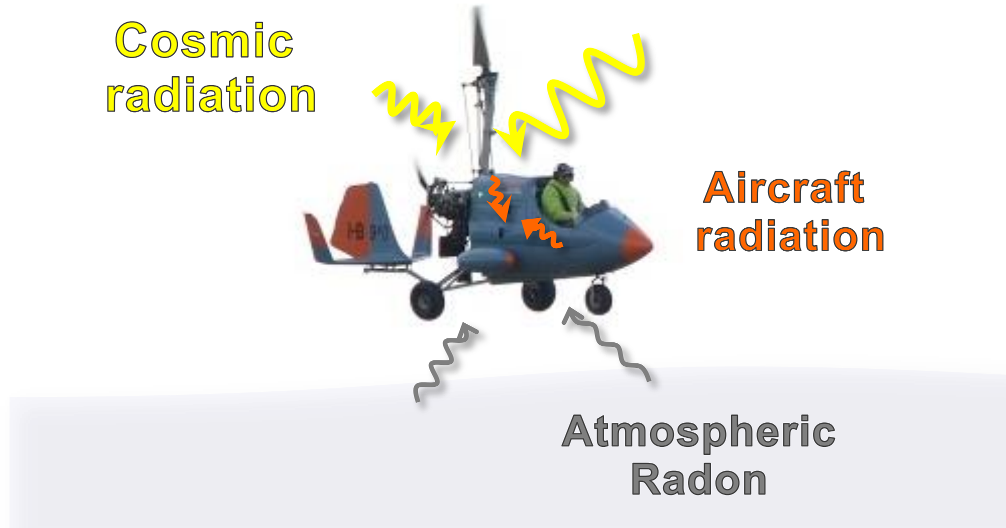

HOW: acquisition of gamma spectra **over water** at **different heights**

- ✓ 4 offshore airborne gamma-ray surveys have been performed for a **~5 hour** acquisition time
- ✓ the **(77 – 3066) m** altitude range has been explored
- ✓ **17612 gamma spectra** have been acquired

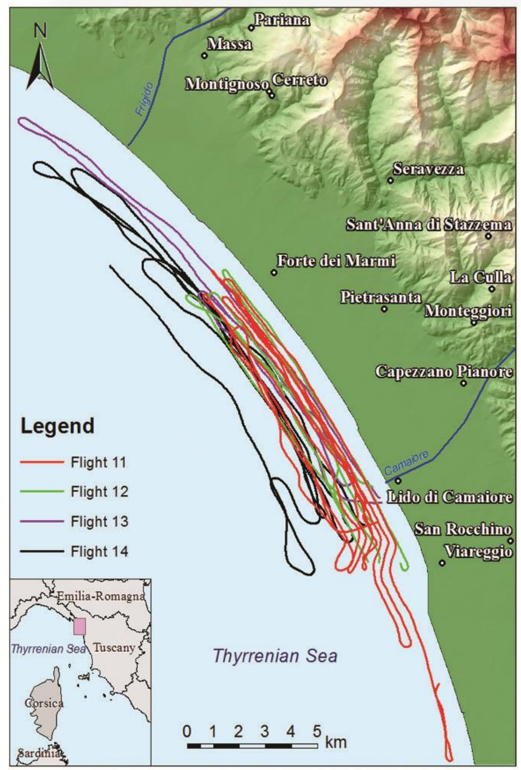

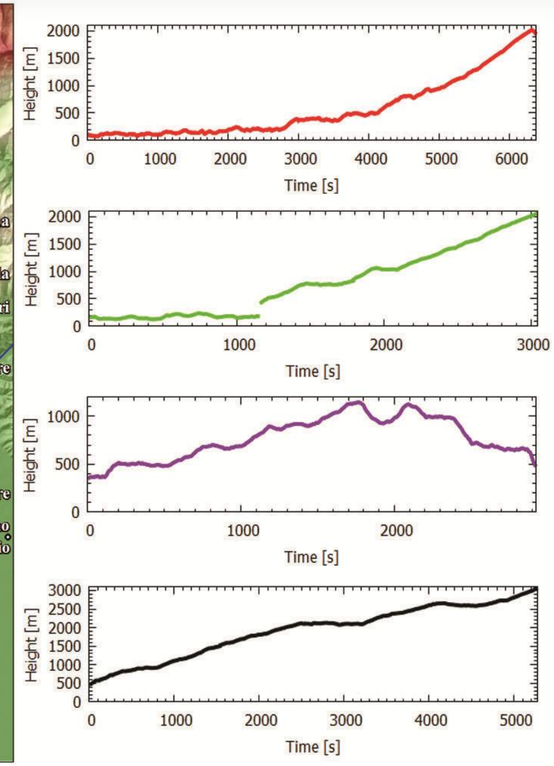

Gamma cosmic radiation and dose

- ✓ At **E>3 MeV** all gamma radiation has **cosmic origin**
- ✓ The gamma component of the cosmic radiation has been measured by monitoring the **Cosmic Energy Window** (CEW) (3 – 7) MeV
- ✓ In the lower atmosphere the intensity of the cosmic gamma radiation **exponentially increases with increasing altitude**

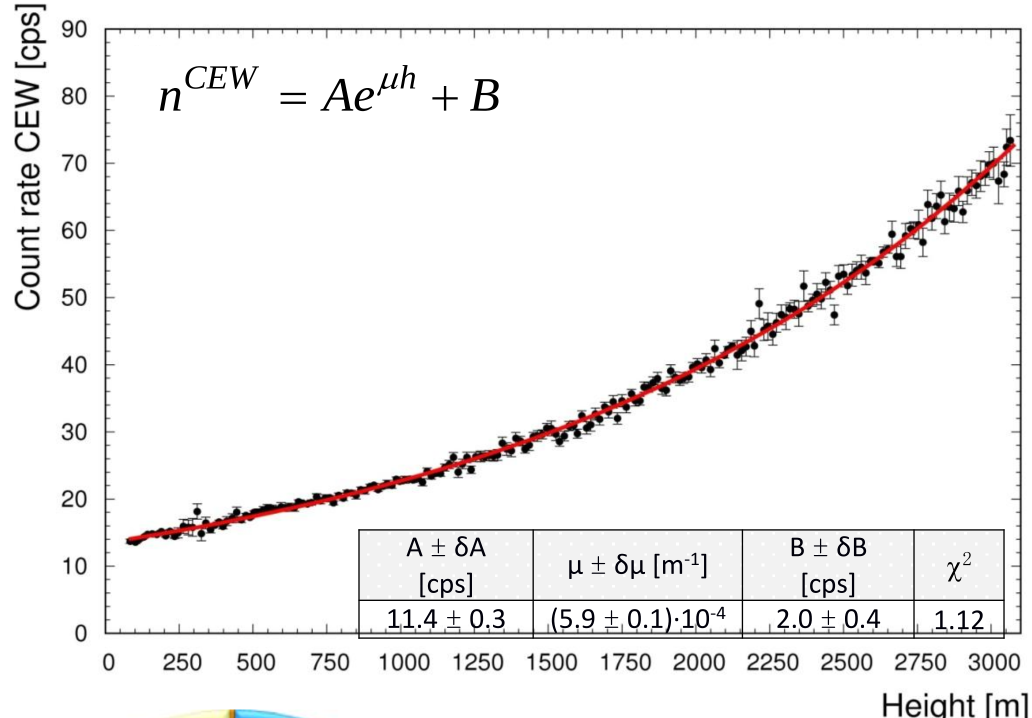

$A \pm \delta A$ [cps]	$\mu \pm \delta\mu$ [m^{-1}]	$B \pm \delta B$ [cps]	χ^2
11.4 ± 0.3	$(5.9 \pm 0.1)\cdot 10^{-4}$	2.0 ± 0.4	1.12

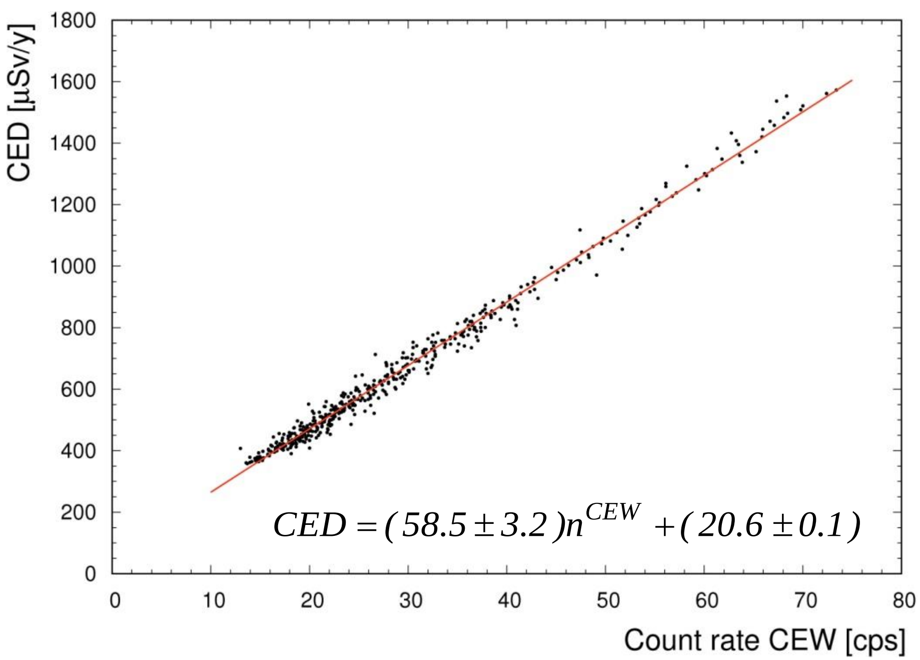

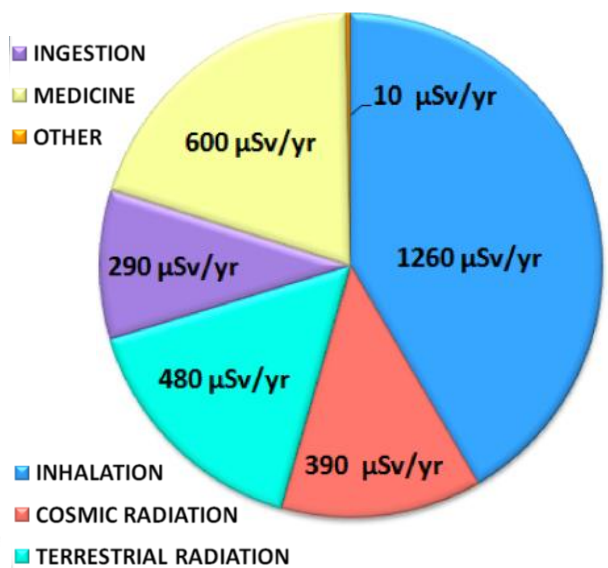

The AGRS detector has been **calibrated** for the **cosmic effective dose** by adopting cosmic dose values provided by the CARI-6 software (US Federal Aviation Administration)

Cosmic spectral shape

✓ The cosmic component of a measured gamma spectrum can be reconstructed in the
Cosmic Energy Window (CEW) (3 – 7) MeV
Natural Energy Window (NEW) (0.8 – 3) MeV

- **CEW**: the counting statistics has pure cosmic nature but the sole reconstruction of the high energy tail is affected by large uncertainties

Energy Window	γ line (MeV)	Energy range (MeV)	Count rate at 2100 m [cps]
Potassium	1.46 (^{40}K)	1.37 – 1.57	0.33
Bismuth	1.76 (^{214}Bi)	1.66 – 1.86	0.27
Thallium	2.61 (^{208}Tl)	2.41 – 2.81	0.15
Cosmic	/	3.00 – 7.00	41.9

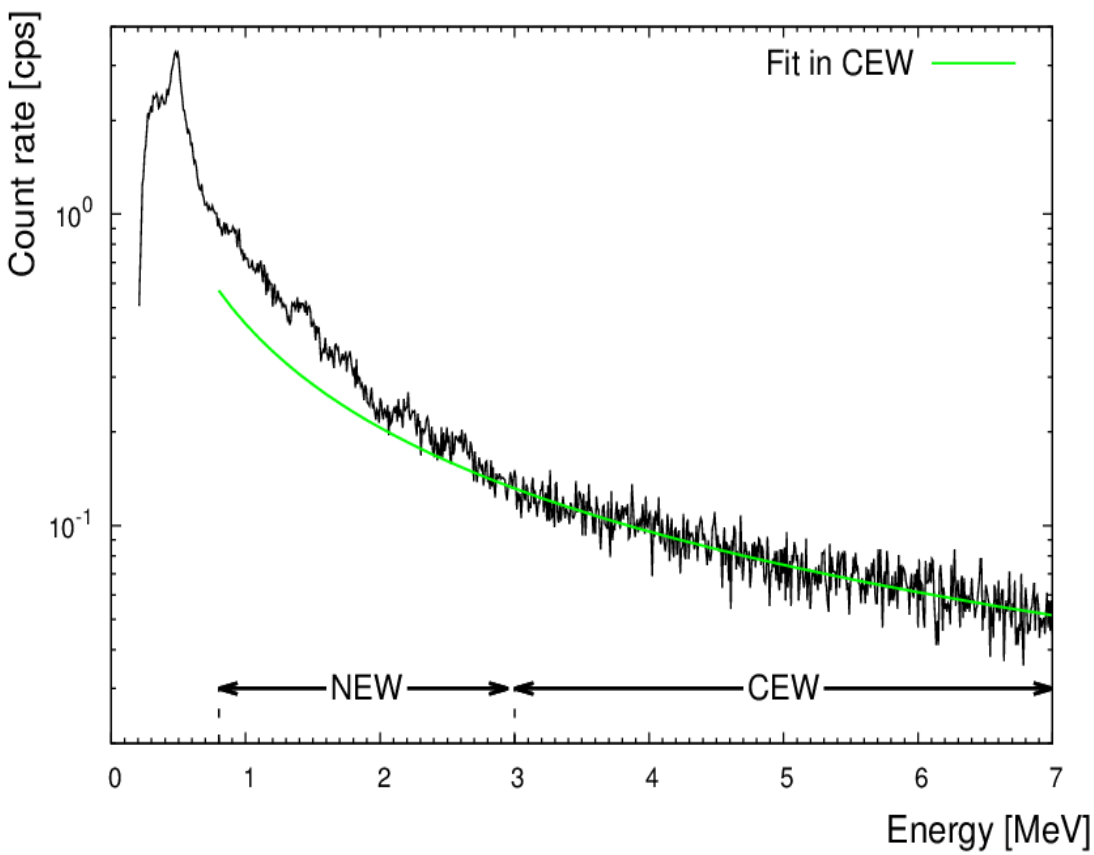

Cosmic spectral shape

✓ The cosmic component of a measured gamma spectrum can be reconstructed in the
Cosmic Energy Window (CEW) (3 – 7) MeV
Natural Energy Window (NEW) (0.8 – 3) MeV

Energy Window	γ line (MeV)	Energy range (MeV)	Count rate at 2100 m [cps]
Potassium	1.46 (^{40}K)	1.37 – 1.57	0.33
Bismuth	1.76 (^{214}Bi)	1.66 – 1.86	0.27
Thallium	2.61 (^{208}Tl)	2.41 – 2.81	0.15
Cosmic	/	3.00 – 7.00	41.9

- **CEW**: the counting statistics has pure cosmic nature but the sole reconstruction of the high energy tail is affected by large uncertainties
- **CEW+NEW**: the ^{40}K, ^{214}Bi and ^{208}Tl points aid constraining the low energy trend of the cosmic shape, necessary to separate the K, U and Th constant aircraft component

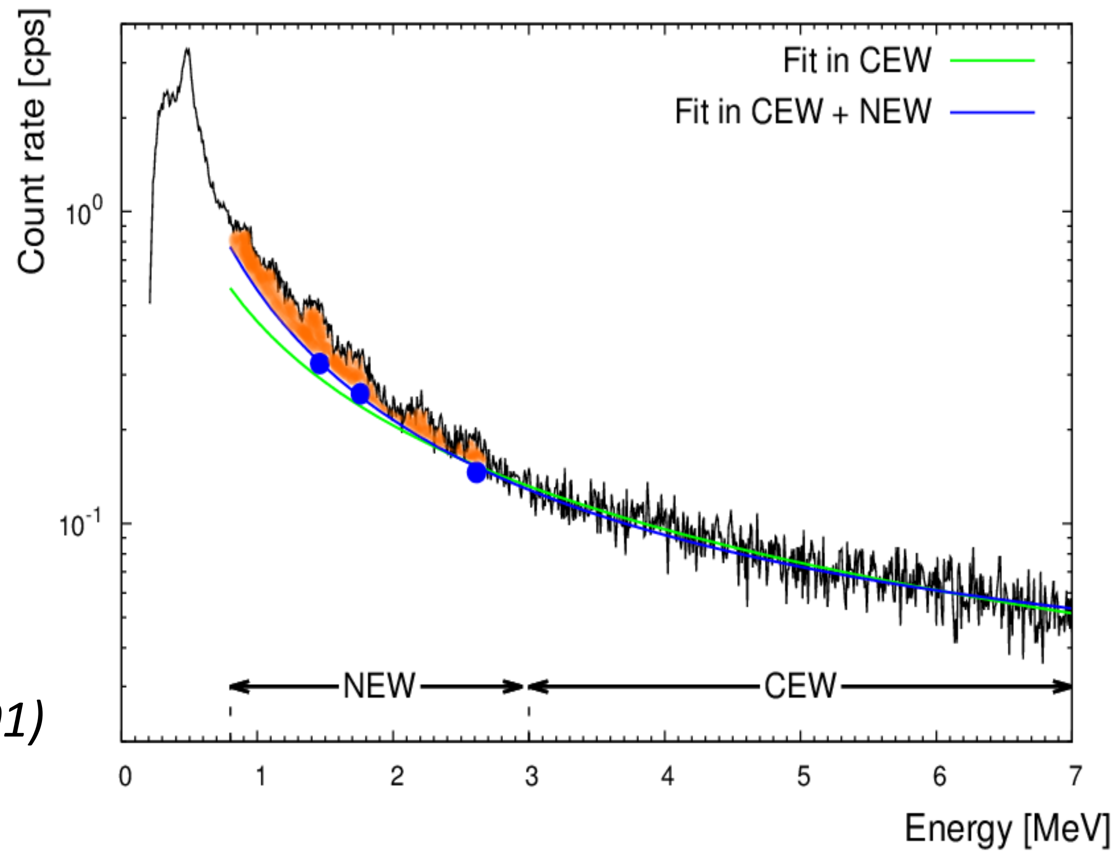

✓ The cosmic spectral shape has been reconstructed at 2100 m as

$$cps = (0.54 \pm 0.04)\, E^{(-1.49 \pm 0.05)} + (0.02 \pm 0.01)$$

Cosmic spectral shape

✓ The cosmic component of a measured gamma spectrum can be reconstructed in the Cosmic Energy Window (CEW) (3 – 7) MeV
Natural Energy Window (NEW) (0.8 – 3) MeV

- **CEW**: the counting statistics has pure cosmic nature but the sole reconstruction of the high energy tail is affected by large uncertainties
- **CEW+NEW**: the ^{40}K,^{214}Bi and ^{208}Tl points aid constraining the low energy trend of the cosmic shape, necessary to separate the K, U and Th constant aircraft component

✓ The cosmic spectral shape has been reconstructed at 2100 m as

$$cps = (0.54 \pm 0.04)\, E^{(-1.49 \pm 0.05)} + (0.02 \pm 0.01)$$

Energy Window	γ line (MeV)	Energy range (MeV)	Count rate at 2100 m [cps]
Potassium	1.46 (^{40}K)	1.37 – 1.57	0.33
Bismuth	1.76 (^{214}Bi)	1.66 – 1.86	0.27
Thallium	2.61 (^{208}Tl)	2.41 – 2.81	0.15
Cosmic	/	3.00 – 7.00	41.9

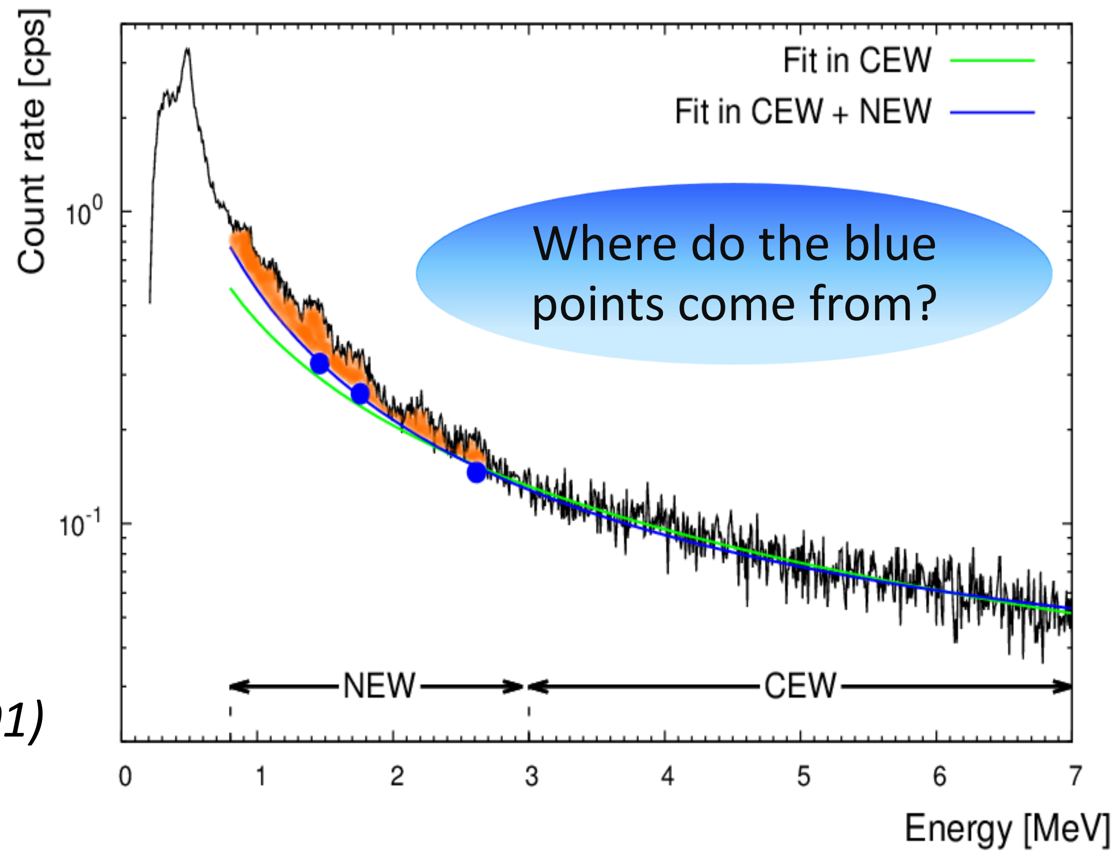

Cosmic background and minimum equivalent abundances

Linear regressions between the count rates in one energy window (^{40}K, ^{214}Bi and ^{208}Tl) and the cosmic count rates provide:

- **b**: **cosmic stripping ratio**
- **a**: constant background count rate due to the **aircraft radioactivity**

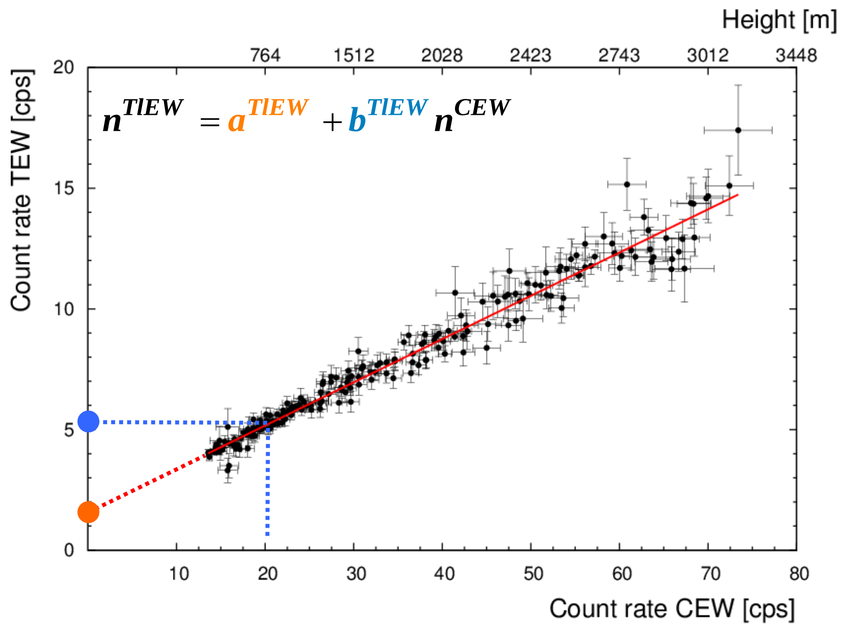

For the first time the **minimum equivalent abundances (MEA)** of **K, U** and **Th** have been calculated

Isotope	MEA	Aircraft cps
K	$0.05 \cdot 10^{-2}$g/g	3.7 ± 0.4
U	0.4 μg/g	2.0 ± 0.4
Th	0.8 μg/g	1.58 ± 0.04

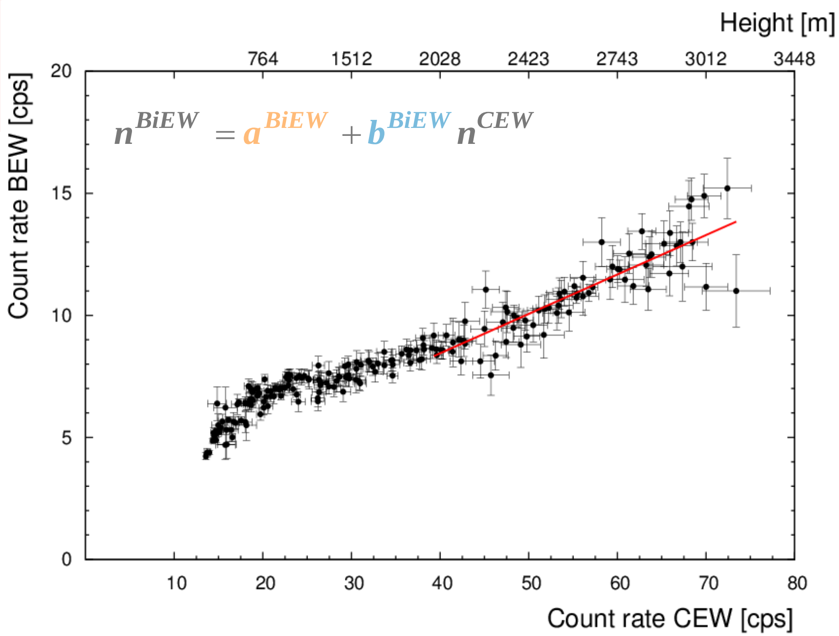

Cosmic background and minimum equivalent abundances

Linear regressions between the count rates in one energy window (^{40}K, ^{214}Bi and ^{208}Tl) and the cosmic count rates provide:

- **b**: **cosmic stripping ratio**
- **a**: constant background count rate due to the **aircraft radioactivity**

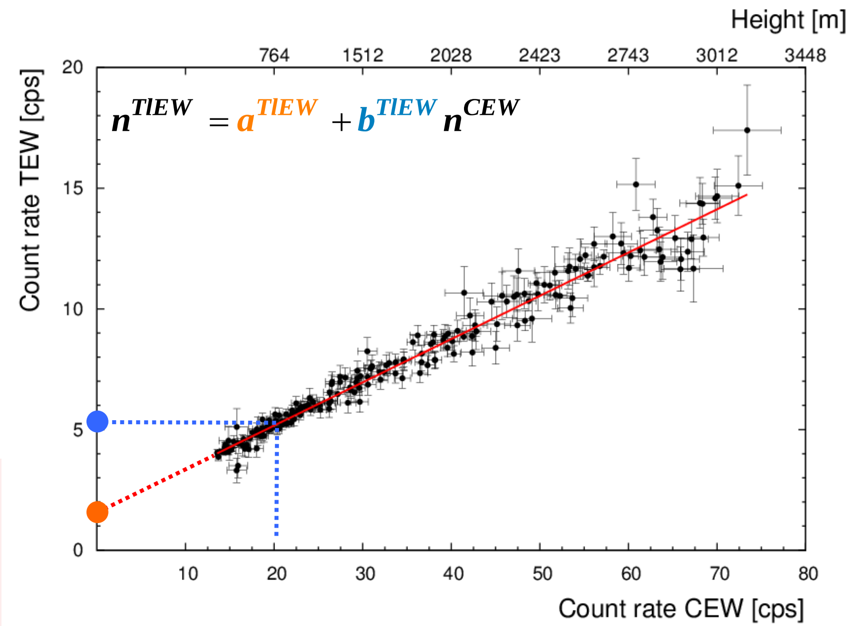

For the first time the **minimum equivalent abundances (MEA)** of **K, U** and **Th** have been calculated

Isotope	MEA	Aircraft cps
K	$0.05 \cdot 10^{-2}$ g/g	3.7 ± 0.4
U	0.4 μg/g	2.0 ± 0.4
Th	0.8 μg/g	1.58 ± 0.04

Workshop on AGRS
Ferrara 8-15 Oct. 2016
Dr. Brian Minty received
Copernicus Visiting Scientist award

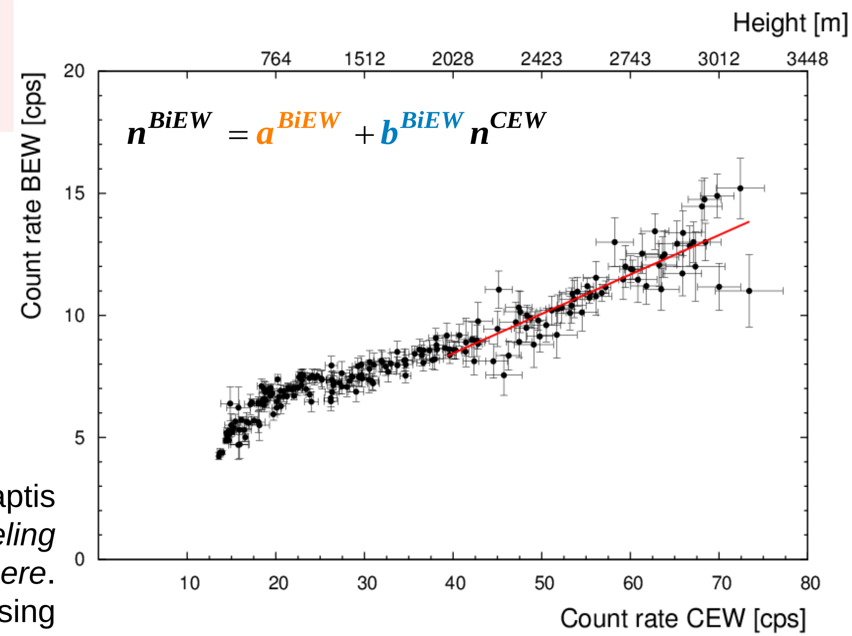

Baldoncini M., Albèri M., Bottardi C., Mantovani F., Minty B., Raptis K., Strati V. *Airborne gamma-ray spectroscopy for modeling cosmic radiation and effective dose in the lower atmosphere*. Submitted to IEEE Transactions on Geoscience and Remote Sensing


New challenges in...
...the spectral reconstruction of...
...terrestrial gamma rays and...
...reactor antineutrinos

^{222}Rn: a phantom gamma background source in the lower atmosphere

✓ ^{222}Rn is the **only gaseous product** of the **^{238}U decay chain**. The relatively long half-life (**$\tau_{1/2}$ = 3.82 days**) allows ^{222}Rn to exhale from soils and rocks and diffuse into the atmosphere

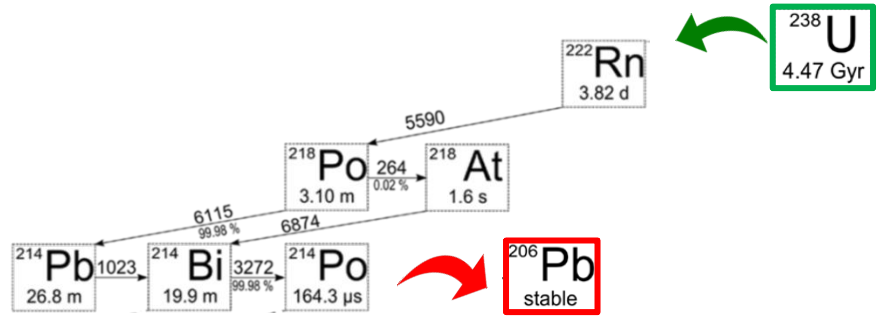

✓ ^{222}Rn is an interesting **natural tracer** for studying processes in the **atmospheric boundary layer** (e.g. vertical air mixing, atmospheric pollutants, climate and chemical transport models)

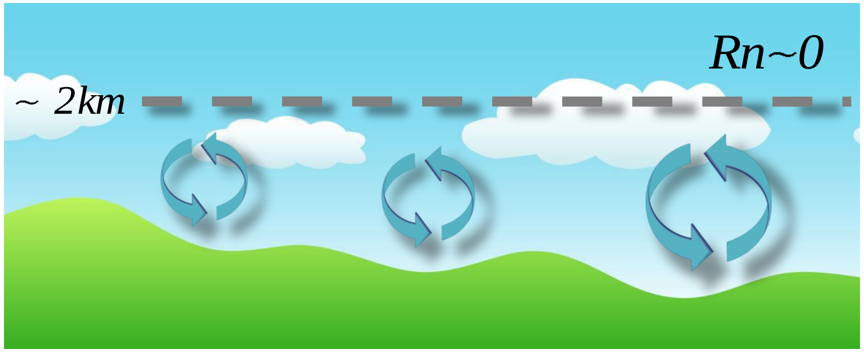

✓ The most prominent gamma-ray emitter (^{214}Bi) occurs below ^{222}Rn: the presence of **^{222}Rn in the atmosphere mimics** the signal due to **^{238}U in the soil**

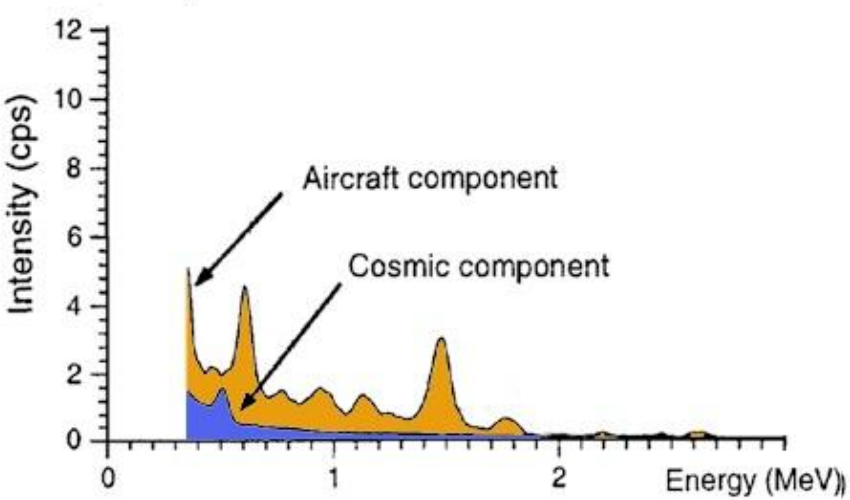

^{222}Rn: a phantom gamma background source in the lower atmosphere

✓ ^{222}Rn is the **only gaseous product** of the **^{238}U decay chain**. The relatively long half-life (**$\tau_{1/2}$ = 3.82 days**) allows ^{222}Rn to exhale from soils and rocks and diffuse into the atmosphere

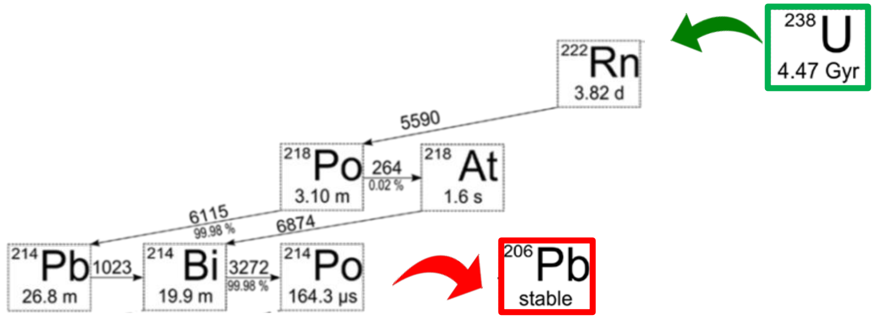

✓ ^{222}Rn is an interesting **natural tracer** for studying processes in the **atmospheric boundary layer** (e.g. vertical air mixing, atmospheric pollutants, climate and chemical transport models)

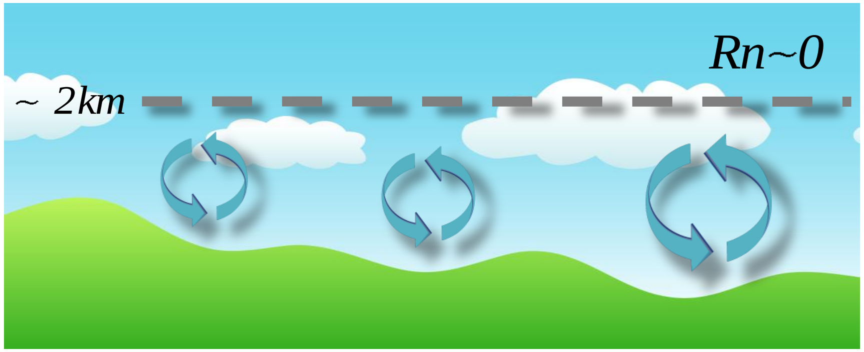

✓ The most prominent gamma-ray emitter (^{214}Bi) occurs below ^{222}Rn: the presence of **^{222}Rn in the atmosphere mimics** the signal due to **^{238}U in the soil**

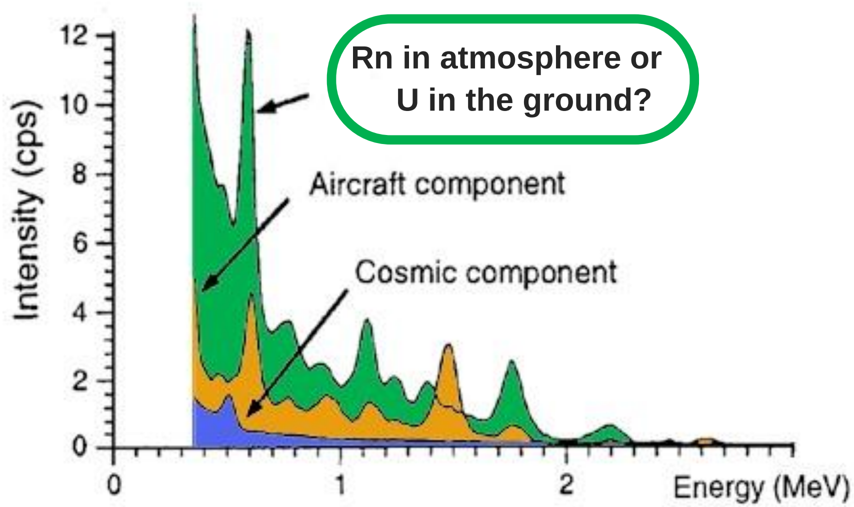

The state of art on ^{222}Rn with AGRS in the lower atmosphere

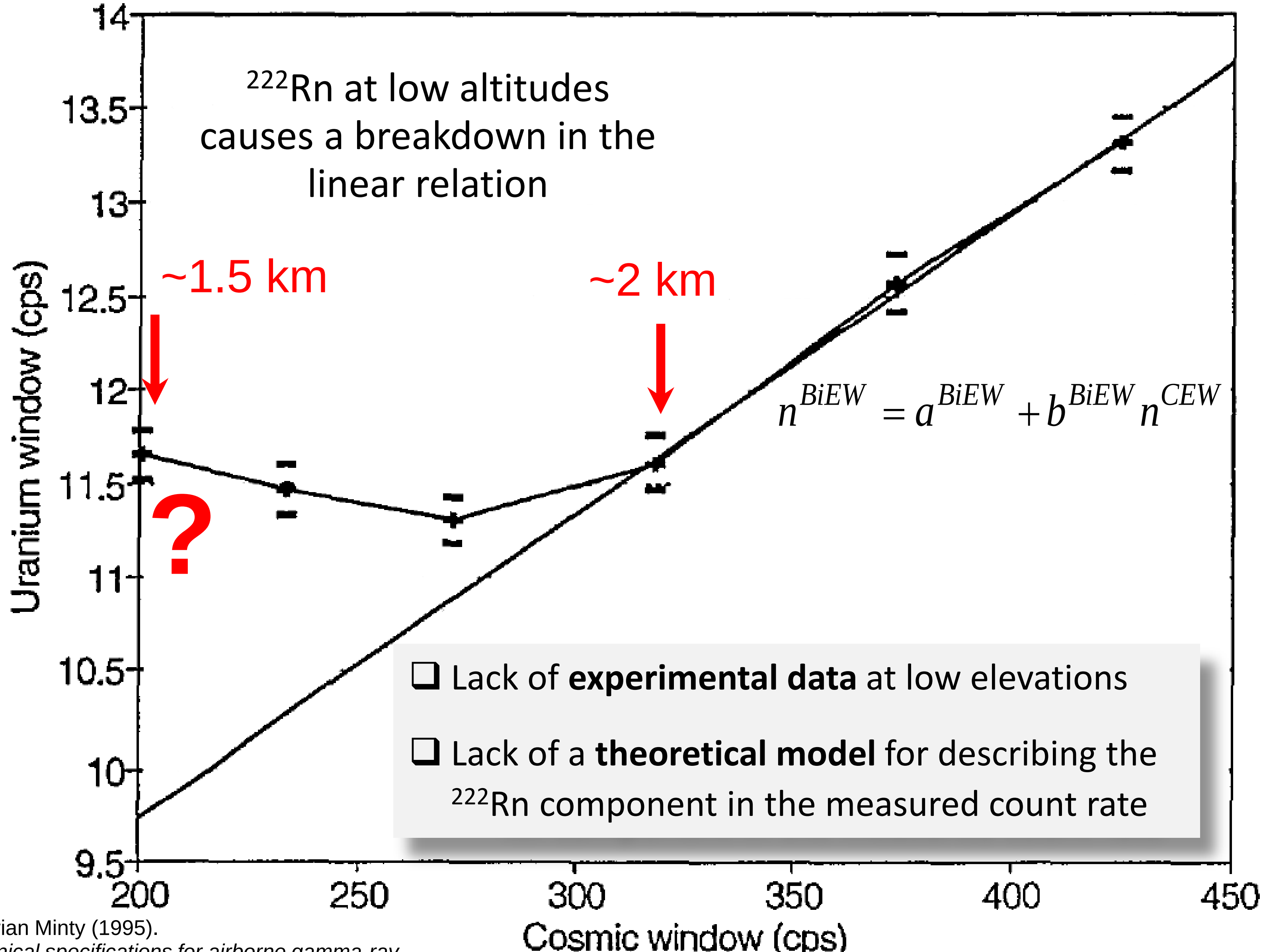

- ❑ Lack of **experimental data** at low elevations
- ❑ Lack of a **theoretical model** for describing the ^{222}Rn component in the measured count rate

Grasty, R.L. and Brian Minty (1995). *A guide to the technical specifications for airborne gamma-ray surveys*. Geoscience Australia

Theoretical model for the ^{222}Rn count rate in the BiEW

The model adopts a **two strata ^{222}Rn vertical profile**

$$a_{Rn} = \begin{cases} \text{Const } (z<s) \\ 0 \ (z>s) \end{cases}$$

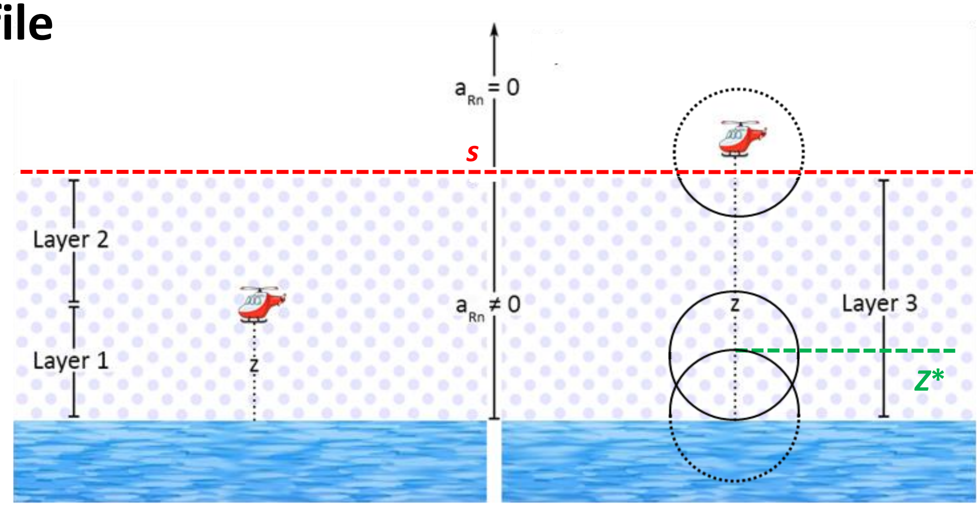

The expected count rate due to atmospheric ^{222}Rn is modeled on the base of ^{214}Bi **unscattered photons propagation**

$$n_{Rn}(a_{Rn},z) = \Theta(s-z)\left[n_1(a_{Rn},z)+n_2(a_{Rn},z)\right]+\Theta(z-s)n_3(a_{Rn},z)$$

$$n_{Rn}(z)=\Theta(s-z)\left[a_{Rn}\int d\cos\theta\left(1-exp\left(-\frac{\mu z}{\cos\theta}\right)\right)+a_{Rn}\int d\cos\theta\left(1-exp\left(-\frac{\mu(s-z)}{\cos\theta}\right)\right)\right]+$$

$$+\Theta(z-s)\left[a_{Rn}\int d\cos\theta\, exp\left(-\frac{\mu(z-s)}{\cos\theta}\right)\left(1-exp\left(-\frac{\mu s}{\cos\theta}\right)\right)\right]$$

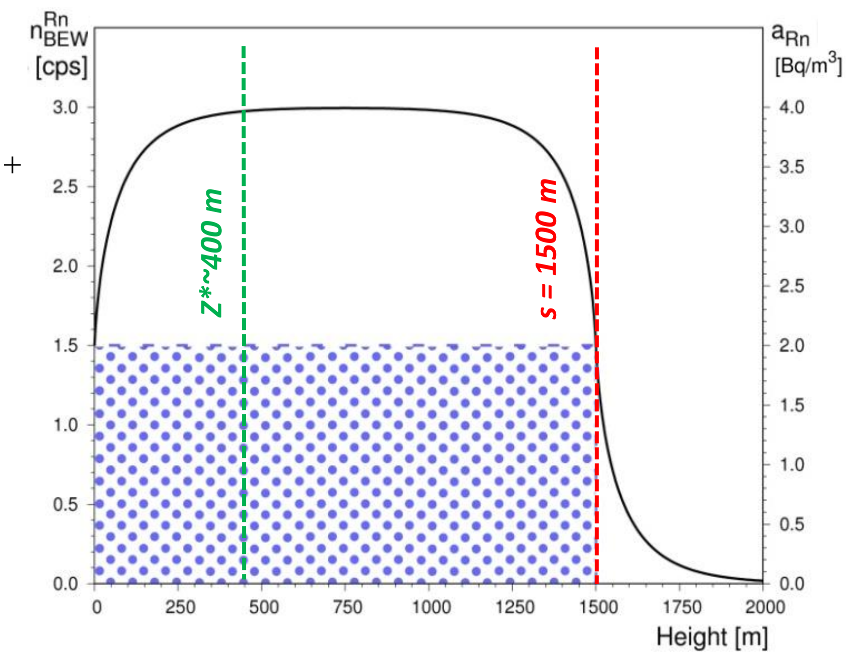

The count rate profile is governed by the ^{214}Bi photon mean free path μ^{-1}, by the ^{222}Rn abundance $\mathbf{a_{Rn}}$ and by the mixing layer depth **s**

^{222}Rn measurement with AGRS

The theoretical model is applied for fitting the experimental count rate in the Bi Energy Window (BiEW), collected in **14688** gamma spectra acquired over the sea in the (**77 – 3066**) m altitude range

A ± δA [cps]	μ ± δμ [m^{-1}]	B ± δB [cps]	$a_{Rn} \pm \delta a_{Rn}$ [Bq/m^3]	s ± δs [m]
8.2 ± 0.2	(2.54 ± 0.0.6)·10^{-4}	-4.9 ± 0.2	0.96 ± 0.07	1318 ± 22

The refined model fits the data better than the standard model and the mean ^{222}Rn concentration and mixing layer depth are in perfect agreement with the data published in literature (a_{Rn} ~ 1Bq/m^3; s ~ 1500 m)

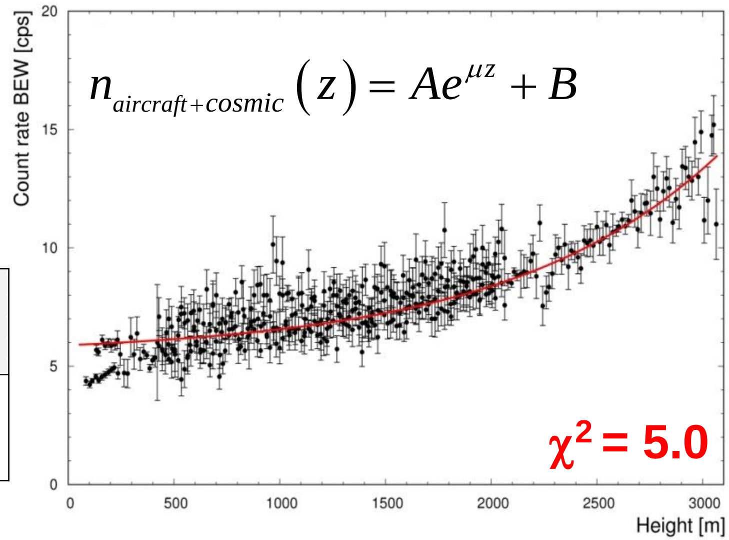

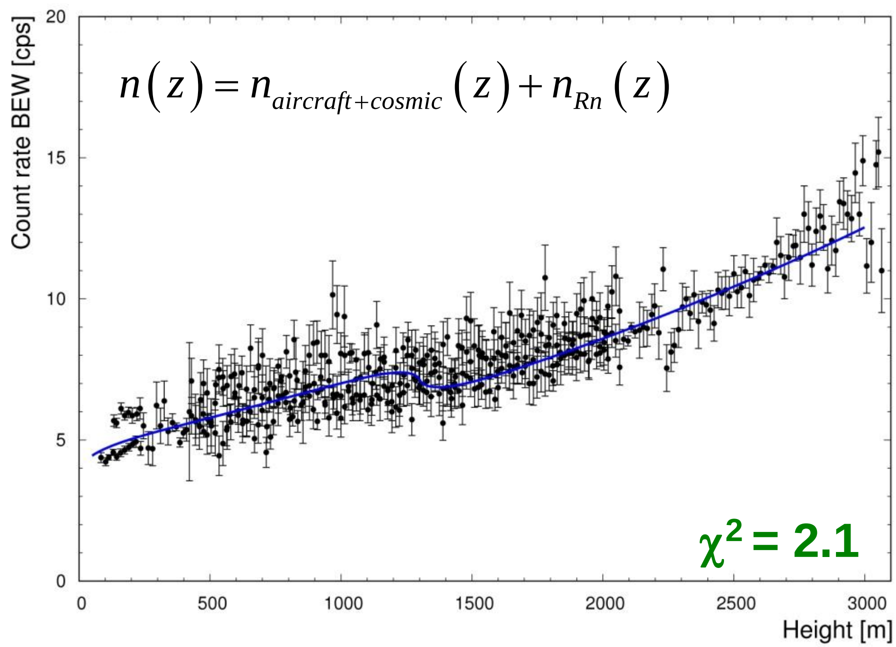

^{222}Rn measurement with AGRS

The theoretical model is applied for fitting the experimental count rate in the Bi Energy Window (BiEW), collected in **14688** gamma spectra acquired over the sea in the (**77 – 3066**) m altitude range

A ± δA [cps]	μ ± δμ [m^{-1}]	B ± δB [cps]	$a_{Rn} \pm \delta a_{Rn}$ [Bq/m^3]	s ± δs [m]
8.2 ± 0.2	(2.54 ± 0.0.6)·10^{-4}	-4.9 ± 0.2	0.96 ± 0.07	1318 ± 22

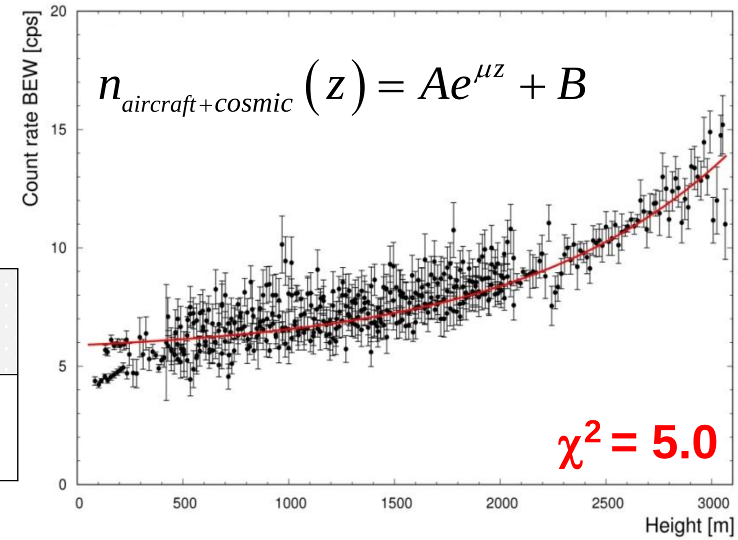

The refined model fits the data better than the standard model and the mean ^{222}Rn concentration and mixing layer depth are in perfect agreement with the data published in literature (a_{Rn} ~ 1Bq/m^3; s ~ 1500 m)

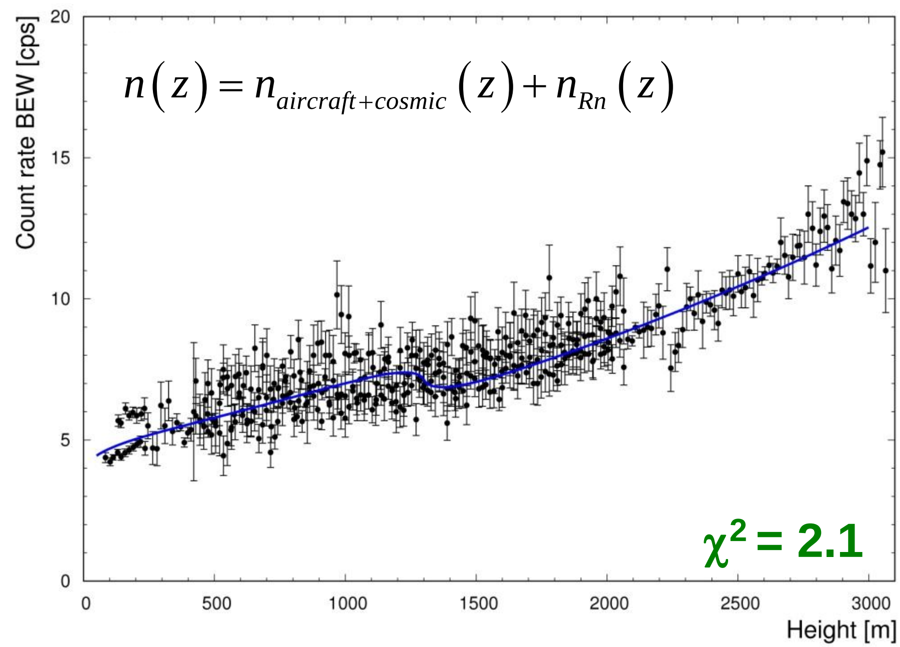

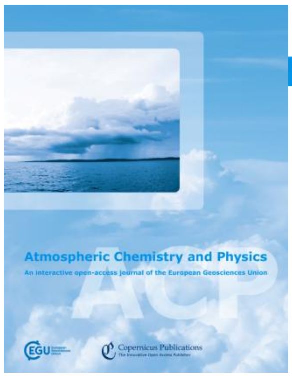

Baldoncini M., Albèri M., Bottardi C., Mantovani F., Minty B., Raptis K., Strati V.
Exploring atmospheric radon with airborne gamma-ray spectroscopy.
Submitted to Atmospheric Chemistry and Physics

CONCLUSIONS

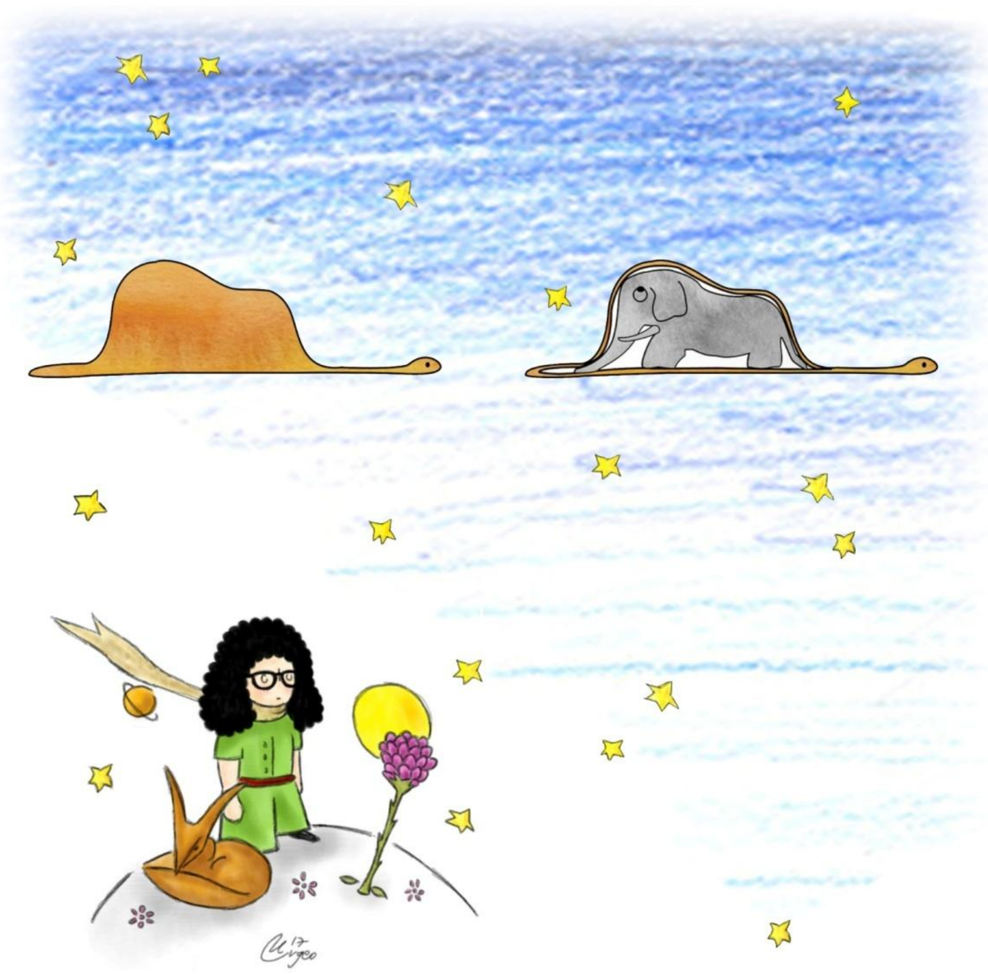

CONCLUSIONS

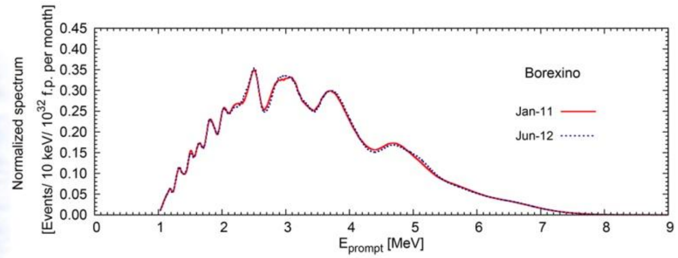

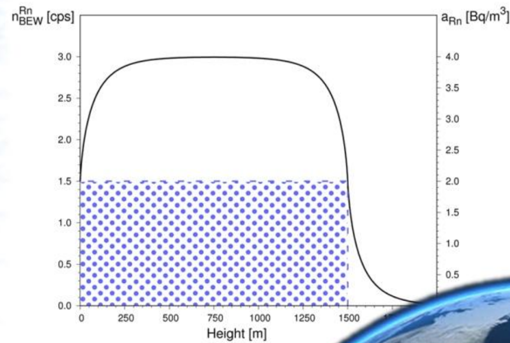

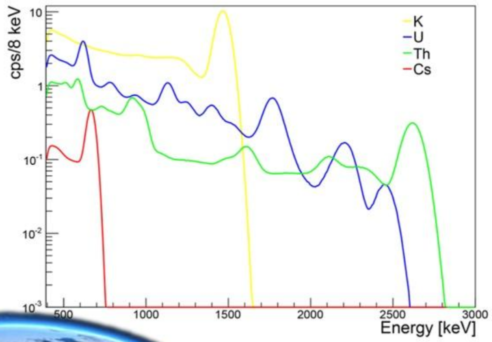

List of publications

Baldoncini M., Albèri M., Bottardi C., Mantovani F., Minty B., Raptis K., Strati V. *Airborne gamma-ray spectroscopy for modeling cosmic radiation and effective dose in the lower atmosphere*. **Submitted to IEEE Transactions on Geoscience and Remote Sensing** **(IF: 3.514)**

Baldoncini M., Albèri M., Bottardi C., Mantovani F., Minty B., Raptis K., Strati V. *Exploring atmospheric radon with airborne gamma-ray spectroscopy*. **Submitted to Atmospheric Chemistry and Physics** **(IF: 5.626)**

KaceliXhixha, M., Albèri, M., **Baldoncini, M.**, Bezzon, G.P., Buso, G.P., Callegari, I., Casini, L., Cuccuru, S., Fiorentini, G., Guastaldi, E., Mantovani, F., Mou, L., Oggiano, G., Puccini, A., Rossi Alvarez, C., Strati, V., Xhixha, G., Zanon, A.. *Map of the uranium distribution in the Variscan Basement of Northeastern Sardinia.* **Journal of Maps** (2015) **(IF: 1.435)**

Xhixha, G., Alberi, **M., Baldoncini**, M., Bode, K., Bylyku, E., Cfarku, F., Callegari, I., Hasani, F., Landsberger, S., Mantovani, F., Rodriguez, E., Shala, F., Strati, V., Kaçeli Xhixha, M. *Calibration of HPGe detectors using certified reference materials of natural origin*. **Journal of Radioanalytical and Nuclear Chemistry** (2015) **(IF: 0.983)**

Xhixha, G., **Baldoncini, M.**, Callegari, I., Colonna, T., Hasani, F., Mantovani, F., Shala, F., Strati, V., and Xhixha Kaceli, M. *A century of oil and gas exploration in Albania: Assessment of Naturally Occurring Radioactive Materials (NORMs).* **Chemosphere** 139, 30-39, (2015) **(IF:3698)**

Baldoncini, M., Callegari, I., Fiorentini, G., Mantovani, F., Ricci, B., Strati, V. and Xhixha, G. *Reference worldwide model for antineutrinos from reactors*. **Physical Review D** 91, 065002 (2015) **(IF: 4.506)**

Strati, V., **Baldoncini, M.**, Bezzon, G. P., Broggini, C., Buso, G. P., Caciolli, A., Callegari, I., Carmignani, L., Colonna, T., Fiorentini, G., Guastaldi, E., Kaçeli Xhixha, M., Mantovani, F., Menegazzo, R., Mou, L., Rossi Alvarez, C., Xhixha, G., and Zanon, A. *Total natural radioactivity, Veneto (Italy).* **Journal of Maps**, 1-7 (2014) **(IF: 1.435)**

Guastaldi, E., **Baldoncini, M.**, Bezzon, G., Broggini, C., Buso, G., Caciolli, A., Carmignani, L., Callegari, I., Colonna T., Dule, K., Fiorentini, G., Kaçeli Xhixha, M., Mantovani, F., Massa, G., Menegazzo, R., Mou, L., Rossi Alvarez, C., Strati, V., Xhixha, G., Zanon, A., *A multivariate spatial interpolation of airborne γ-ray data using the geological constraints*. **Remote Sensing of Environment**, 137 (2013) 1-11 **(IF: 5.881)**

Caciolli, A., **Baldoncini, M.**, Bezzon, G.P., Broggini, C., Buso, G.P., Callegari, I., Colonna, T., Fiorentini, G., Guastaldi, E., Mantovani, F., G. Massa, R. Menegazzo, L. Mou, C.R. Alvarez, M. Shyti, A. Zanon, G. Xhixha, *A new FSA approach for in situ γ ray spectroscopy*. **Science of The Total Environment**, 414 (2012) 639-645 **(IF: 3.976)**